Present-day 3D GPS velocity field of the Iberian Peninsula and implications for seismic hazard

Sara Pena Castellnou

Supervised by: Giorgi Khazaradze

MSc in Mineral Resources and Geological Hazards
Specialty: Geological Hazards

June 2018

UNIVERSITAT DE BARCELONA

UAB
Universitat Autònoma de Barcelona

ABSTRACT

We present a 3D crustal deformation velocity field of the Iberian Peninsula based on the analysis of more than 400 continuous GPS station data from the last 3.3 years (2015-2018 interval) distributed throughout the Iberian Peninsula, northern Africa and southern France. We describe the procedures followed to obtain a combined uniform velocity solution from daily GPS data using GAMIT/GLOBK software. Until now the previously published studies have estimated the 2D horizontal velocity field of the study area, since the vertical component is more complicated to derive. Only the studies by Serpelloni et al. (2013) and Nguyen et al. (2016) have calculated the vertical rates of deformation in some limited areas of the peninsula. In the present work, we provide the main results in terms of the velocity vectors in horizontal and up/down directions. The calculated GPS velocities range from 0.0 to 4.5 mm/yr, in Eurasia fixed reference frame, indicating that the Iberian Peninsula presents a heterogeneous present-day crustal deformation field, which can be grouped into 7 distinct domains/blocks. Each domain is influenced by the geo-tectonic structural configuration of the Iberian Peninsula and by the proximity to the Iberia-Nubia plate boundary. The highest velocities, as well as the highest geodetic strain rates, are detected in the EBSZ and along the Iberia-Nubia plate boundary, areas with the highest seismicity rates. The obtained vertical GPS velocities are preliminary and a processing of extended time-series (from 2010 to present) and more careful treatment of various phenomena affecting the GPS vertical signal (e.g. ocean and tide loading) should be performed in order to better resolve them. However, when the rates of observed vertical rates are high (>10 mm/yr), our results do indicate real motions, for example a subsidence of 6 cm/yr in Guadalentín basin, caused by the groundwater extraction. This kind of information is useful for multi-risk analysis since it can provide information of ongoing uplift/subsidence motion, that can be caused by faults, landslides, sediment settlement and/or anthropogenic activities (e.g. groundwater withdrawal, mining).

***Key words**: Iberian Peninsula, GPS, geodynamics, 3D velocity field, strain rate.*

RESUM

En aquest treball es presenta el camp de velocitats 3D de la Península Ibèrica basat en l'anàlisi de dades obtingudes durant 3,3 anys (des del 2015 al 2018) per més de 400 estacions contínues de GPS distribuïdes per tota la Península Ibèrica, nord d'Àfrica i sud de França, emprant el software GAMIT/GLOBK. Fins ara, tots els estudis geodèsics previs realitzats en la zona d'estudi han estimat el camp horitzontal de velocitats 2D sense calcular la component vertical a causa de la dificultat que suposa processar-la i obtenir-la. No obstant això, Serpelloni et al. (2013) i Nguyen et al. (2016) han derivat i obtingut diversos vectors de velocitat vertical en determinades àrees de la Península. Les velocitats horitzontals calculades en aquest treball varien d'entre 0,0 a 4,5 mm/any, en el sistema de referència que considera Euràsia com a placa fixa, indicant que la Península Ibèrica presenta un actual camp de velocitats heterogeni que pot ser agrupat en 7 dominis ben diferenciats. Cada domini està influenciat per la configuració geotectònica i estructural de la Península i per la proximitat al límit de plaques entre Ibèria i Núbia. Les velocitats més elevades, així com les àrees amb major deformació, es troben a l'EBSZ i al llarg del contacte entre Núbia i Ibèria, que són àrees amb elevada activitat sísmica. El camp de velocitats verticals GPS obtingut és preliminar; per tal de millorar-lo i obtenir una solució coherent és necessari el processament d'un període temporal més llarg (que inclogui més quantitat de dades) i tractar acuradament els diferents fenòmens que afecten la component vertical del senyal GPS (ex. marees i carrega oceànica). No obstant això, quan la taxa de deformació és elevada (>10 mm/any), els resultats obtinguts representen moviments reals; per exemple els 6 cm/anys de la taxa de subsidència a la conca del Guadalentín, causada per l'explotació d'aigua subterrània procedent de l'aqüífer. Aquest tipus d'informació es útil per anàlisis multirisc, proporcionant taxes d'aixecament/subsidència causada per l'activitat de falles, esllavissades, assentament del terreny i/o activitats antròpiques (ex. extracció d'aigua subterrània, mineria).

***Paraules clau**: Península Ibèrica, GPS, geodinàmica, camp de velocitats 3D, taxes de deformació.*

Contents

1. Introduction

The Iberian Peninsula is part of the plate boundary zone that accommodates the relative motion between Africa (Nubia) and Eurasian plates in Western Mediterranean area. It is characterized by a moderate and wide-spread level of seismic activity, mainly concentrated in the Betic and Pyrenees mountain ranges, located respectively in the SE and NE of the Iberian Peninsula. Due to the very slow crustal deformation rates that occur in this area, it is convenient to use GPS technology in order to identify slow moving faults, leading towards a better seismic hazard understanding, since this technique can detect movements inferior to 1 mm/yr.

Global Navigation Satellite System (GNSS) and in particular Global Positioning System (GPS) technology provides a competent tool for studying the kinematics of contemporary crustal deformation of the earth's crust at various scales and precisions. As a consequence of GPS studies realized during the last decade, it has been possible to update global plate motions models, as well as, to identify tectonically active faults and evaluate their seismic potential.

We present the 3D velocity field of the Iberian Peninsula, based on the analysis of the continuous GPS stations scattered throughout the Iberian Peninsula, northern Morocco and southern France and covering a period of 3.3 years (2015 to present day). The main objective of this study is to determine velocity rates using continuous GPS observations in order to identify areas with active deformation and link the obtained results with geological and anthropogenic processes.

Previous related studies in the Iberian Peninsula (Stich et al. 2006; Fernandes et al. 2007; Serpelloni et al. 2007; Khazaradze et al. 2014a; Garate et al. 2015; Palano et al. 2015) have only focused on calculating the 2D velocity field. Only two studies until now have presented vertical deformation rates of the CGPS stations of the peninsula: Serpelloni et al. (2013) presented the first contemporary crustal deformation vertical velocities in the Euro-Mediterranean region, including 114 stations from the Iberian Peninsula, but only covering the central and southeastern regions. The other more recent study was carried out in the Pyrenees and the French Alps (Nguyen et al. 2016), including 27 stations from the Iberian peninsula, concentrated in the Pyrenees.

The paper is organized as follows: section 2 describes the seismotectonic setting of the area that covers this study, section 3 compiles previous geodetic studies that have been carried out in the Iberian Peninsula, section 4 states the methodology by giving an introduction to GPS system, and describing the GPS stations available and how we performed the data processing, section 5 describes the general features of the obtained 3D velocity field and geodetic strain rate maps, in section 6 a discussion of the estimated velocity field is giving as well as its applications in seismic hazard assessment.

2. Seismotectonic setting

2.1 Tectonic evolution

The Iberian Peninsula forms part of the Eurasian tectonic plate and its located at the western end of the Himalayan-Alpine collision zone, dominated by the convergence of the Eurasia and Nubia tectonic plates which takes place at rates of 4.5-5.6 mm/yr, with approximately NW-SE to WNW-ESE shortening direction (DeMets et al. 1994; Argus et al. 2011). The current tectonic plate setting of the Iberian Peninsula has changed significantly due to a complex geo-tectonic evolution throughout its geologic history (Figure 1) that lead to the formation of three major geotectonic units: the Iberian Massif, Alpine chains (e.g. Pyrenees, Iberian Cordillera, Betic Cordillera) and Tertiary basins (e.g. Ebro basin, Guadalquivir basin).

The Iberian plate behaved independently during Cretaceous time (Srivastava et al. 1990). In the Upper Cretaceous the occurrence of different events started triggering the current configuration of Iberia, Eurasia and Nubia tectonic plates and its different affiliations. These were the evolution of the western end of the Tethys and the gradual opening of the North Atlantic Ocean Ridge 120 Ma ago (Sanz de Galdeano 2000).

The continuous oceanic spreading of the North Atlantic Ocean Ridge induced along the northwestern margin of Iberia the opening of the Bay of Biscay (around 115 Ma ago) encompassed by an anti-clockwise rotation of Iberia with respect to Europe (Savostin et al. 1986) producing the collision and Late Cretaceous subduction of the Lingurian Basin on to the eastern side of Iberia (de Jong 1990) (Figure 1). The new dynamic setting led to a clockwise rotation of Eurasia with respect to Iberia causing N-S convergence (onset Alpine orogeny) (Andeweg 2002). The continued moving of Nubia towards the north pushed Iberia leading a continental collision and producing the Pyrenees along the limit with Eurasia.

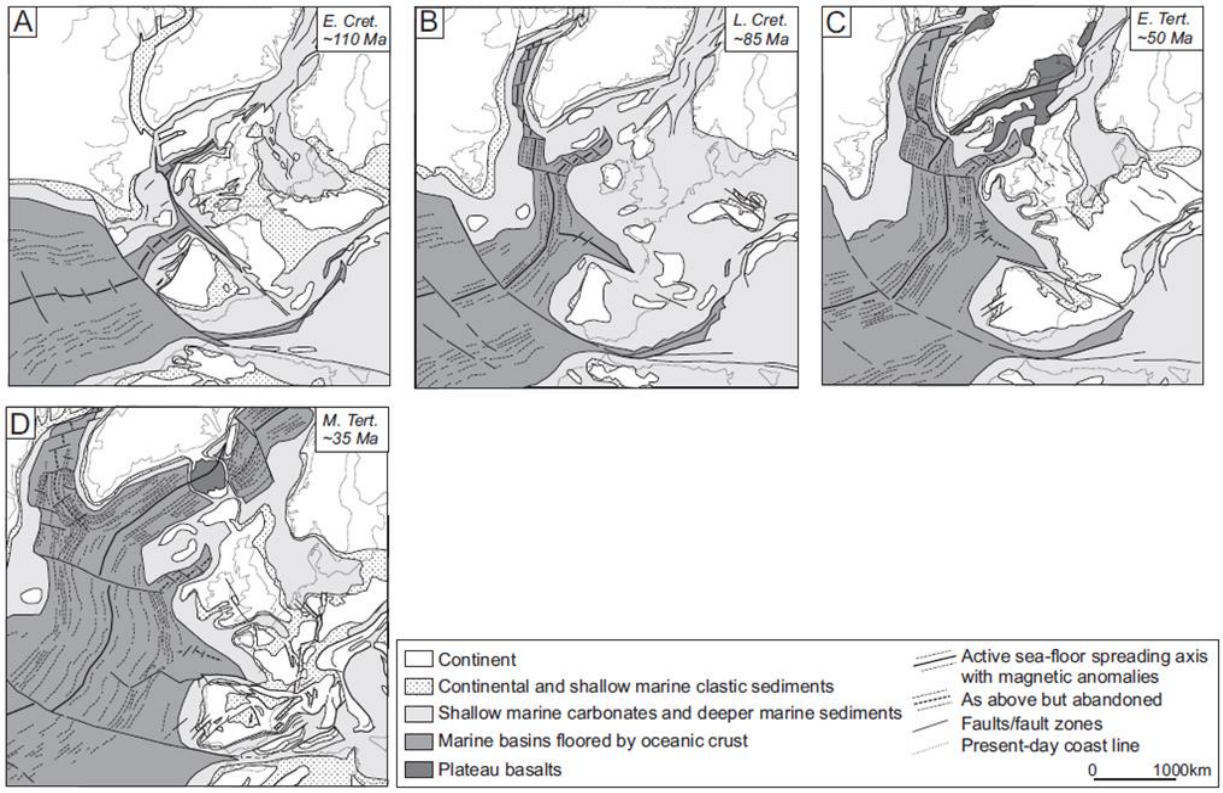

Figure 1: Tectonic evolution of the Iberian Peninsula due to the progressive opening of the North Atlantic causing several periods of differential motion between the Eurasian, Nubia, and Iberian plates. A = Early Cretaceous (~110 Ma), B = Late Cretaceous (~85 Ma), C = Early Tertiary (~50 Ma) and D = Middle Tertiary (~35 Ma). (Andeweg 2002).

In contrast to the Mesozoic, during the Tertiary and Quaternary periods the Iberian Peninsula was dominated by compressional deformation, accompanied by simultaneous E-W extension affecting Central Europe since the Eocene, and later reaching the Western Mediterranean (Andeweg 2002). Most of the Pyrenean shortening was completed by middle Oligocene times and since then the convergence of Nubia was mostly accommodated across the Atlas systems (North Africa), the Betic-Rif orogenic system and within the Iberian Peninsula, inverting all previously rifted regions and producing intraplate mountain ranges, like the Iberian Chain and Catalan Coastal Ranges (Vergés and Fernàndez 2012).

Further southwards, the Valencia Trough and Balearic Basin opened leading to the formation of the Betic-Rift arc (Rosenbaum et al. 2002). This extensional process occurring in the western Mediterranean together with the constant eastward drift of Iberia due to Atlantic opening, compressed the eastern sector of Iberia in approximately E-W direction (Sanz de Galdeano 2000) which triggered the activation of the left lateral Azores-Gibraltar zone in the south of Iberia becoming the active boundary between Nubia and Eurasia (Srivastava et al. 1990). At the end of the Early Miocene the formation of the Pyrenees was completed and the Iberian plate was merged with the Eurasian plate (Srivastava et al. 1990).

Present day limit of Eurasia and Nubia plate is embraced by the left lateral Azores-Gibraltar zone. This limit is diffused (Stich et al. 2003) containing the Betic Cordillera in southern Iberia, the Rif and Tell mountains in northwestern Africa and the Alboran Sea in between (together forming the Gibraltar Arc).

In the Iberian Peninsula, the most actively deforming zone corresponds to the Eastern Betic Shear Zone (EBSZ), located in the southeast. The EBSZ is an area of 400 km wide which absorbs part of the present 4.5-5.6 mm/yr shortening (DeMets et al. 1994; Argus et al. 2011) between the European and African plates in this area (Masana et al. 2004). It is composed of an active system of left-lateral strike-slip faults producing low to moderate magnitude shallow earthquakes, although large historical events have also occurred in the past (Mezcua et al. 2013).

2.2 Seismicity

The Iberian Peninsula has a moderate seismic activity mainly concentrated along the southern part, the Pyrenees and the northwestern area (Galicia). Therefore the Betic Cordillera and North Morocco are the most active areas (Figure 2). As can be seen, all the borders of the Iberian Peninsula are characterized by a diffuse seismicity, while on the central sector seismicity wanes.

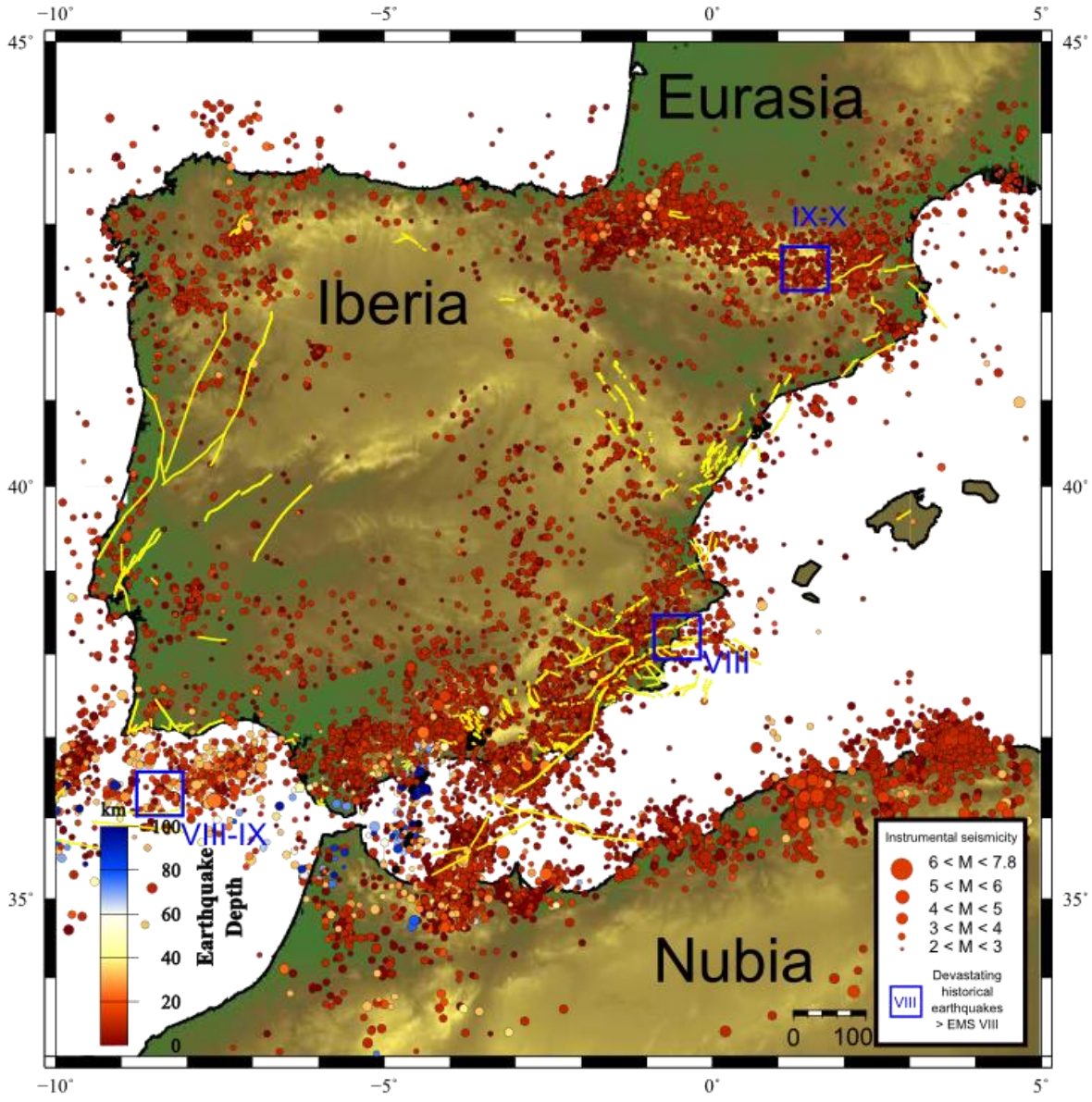

Figure 2: Instrumental seismicity of the Iberian Peninsula during the 1964-2018 time period. The earthquakes are from USGS seismic catalogue (https://earthquake.usgs.gov). Yellow lines correspond to faults that have been active during the Quaternary period. These were retrieved from QAFI database (http://info.igme.es/qafi).

The seismicity in the southern part of the peninsula is related to kinematics of the Nubia-Eurasia plate boundary and it's widely spread. Bufforn (2004) identifies 3 areas with different behavior: A) the Gulf of Cadiz, B) Betics, Alboran Sea and northern Morocco and C) Algeria. In the A area epicenters are distributed in an E-W direction, across a band about 100 km wide with focus at shallow and intermediate depth with events, in general, of less than Mw 5.5. Highlights the Lower Tajo Valley, near Lisbon (Portugal)

for high activity (Buforn et al. 2004). In the B area there are three main concentrations of epicenters: northern Morocco, Almeria region and Granada Basin with events ranging Mw 5 (Buforn et al. 2004). In the C area epicenters are concentrated in Algeria where earthquakes with magnitude higher than 6 occurred (Buforn et al. 2004). An important feature of the seismicity of this region is the occurrence of very deep earthquakes (shown in black in Figure 2). These are the deepest earthquakes in the Mediterranean region occurring in the uppermost continental mantle linked with a subducted slab nevertheless this hypothesis is still a debate (Buforn et al. 2011).

In the Pyrenees seismicity is low-moderate with frequent occurrence of earthquakes with Mw>2 and mainly concentrated in the western part. Although in this region the instrumental seismicity is moderate, the historical seismicity is high. A number of ten earthquakes of intensity MSK>VIII and four MSK=IX occurred denoting the seismic potential of this area (Asensio 2014). The northwestern part of the Iberian Peninsula shows a permanent seismicity of low to moderate magnitude compared to the seismotectonic context of the Euro-Mediterranean region. However, several crises have occurred in Lugo province, with a main earthquake of magnitude 5.3 in 1997 (López-Fernández et al. 2008).

In terms of the historical seismicity, since the 14th century the Iberian Peninsula has experienced at least 27 EMS98 ≥ VIII intensity earthquakes (Mezcua et al. 2013) including the devastating Lisbon earthquake of 1755 (EMS VIII-IX), 1829 Torrevieja (Alicante, EMS VIII) and 1428 Queralbs (Girona, EMS IX-X) earthquakes (Figure 2). However, as mentioned, the instrumental seismicity records (covering a period of time from 1950 to present day) show no major (EMS > VII) crustal type earthquakes recorded in the area.

The most recent damaging earthquake that occurred in Spain, was the Mw 5.1 (2011) Lorca earthquake (Martínez-Díaz et al. 2012), that occurred in SE of the Iberian Peninsula as result of a slip on the Alhama de Murcia fault (belonging to EBSZ).

2.3 Focal mechanisms

The direction of slip, along a fault plane during an earthquake, responds to the stress conditions at the source location. Thus, earthquakes sample the present-day tectonic stress field. Therefore earthquake focal mechanisms are valuable and widely used stress indicators (de Vicente et al. 2008).

Figure 3 shows the distribution of the different stress regimes that occur in the Iberian Peninsula. Over a large part of the Iberian Peninsula, in an intraplate setting, normal faulting mechanisms occur with NE-SW orientation perpendicular to the convergence direction (Stich et al. 2003). Near the southern coast of Portugal strike-slip and reverse mechanisms show consistent orientation with an NNW-SSE direction (Stich et al. 2003; 2010). In the Alboran Sea mechanisms are predominantly strike-slip with nearly N-S orientated P axes and nearly E-W oriented T axes. Most mechanisms include a minor component of normal faulting consistent with the observed regional extension (Stich et al. 2003). Within the Betic Cordillera faulting style changes from predominately strike-slip in the east Betic shear zone towards predominately normal faulting in the central Betics (Stich et al. 2010) with several orientations but predominately NW-SE (de Vicente et al. 2008). In the Pyrenees mechanisms show an extensive regime with NNE-SSW orientated T axes perpendicular to the orientation of the orogenic chain (Stich et al. 2010).

3. Previous geodetic studies

Several geodetic studies were carried out in the Iberian Peninsula, most of them focused on the Iberian-Maghrebi region with the aim of characterizing the present-day boundary between Nubia and Iberia tectonic plates. Fernandes et al. (2003), McClusky et al. (2003) and Nocquet and Calais (2004) calculated the relative motion between Africa and Eurasia from GPS data. Later studies derived the 2D velocity field of the peninsula (Stich et al. 2006; Fernandes et al. 2007; Serpelloni et al. 2007; Vernant et al. 2010; Koulali et al. 2011; Palano et al. 2013, 2015; Khazaradze et al. 2014a; Garate et al. 2015). Also, two PhD thesis have been carried out at the University of Barcelona: Asensio (2014) who focused on the Pyrenees and the Betic Mountain belts and Echeverria (2015) who calculated the deformation field of the EBSZ.

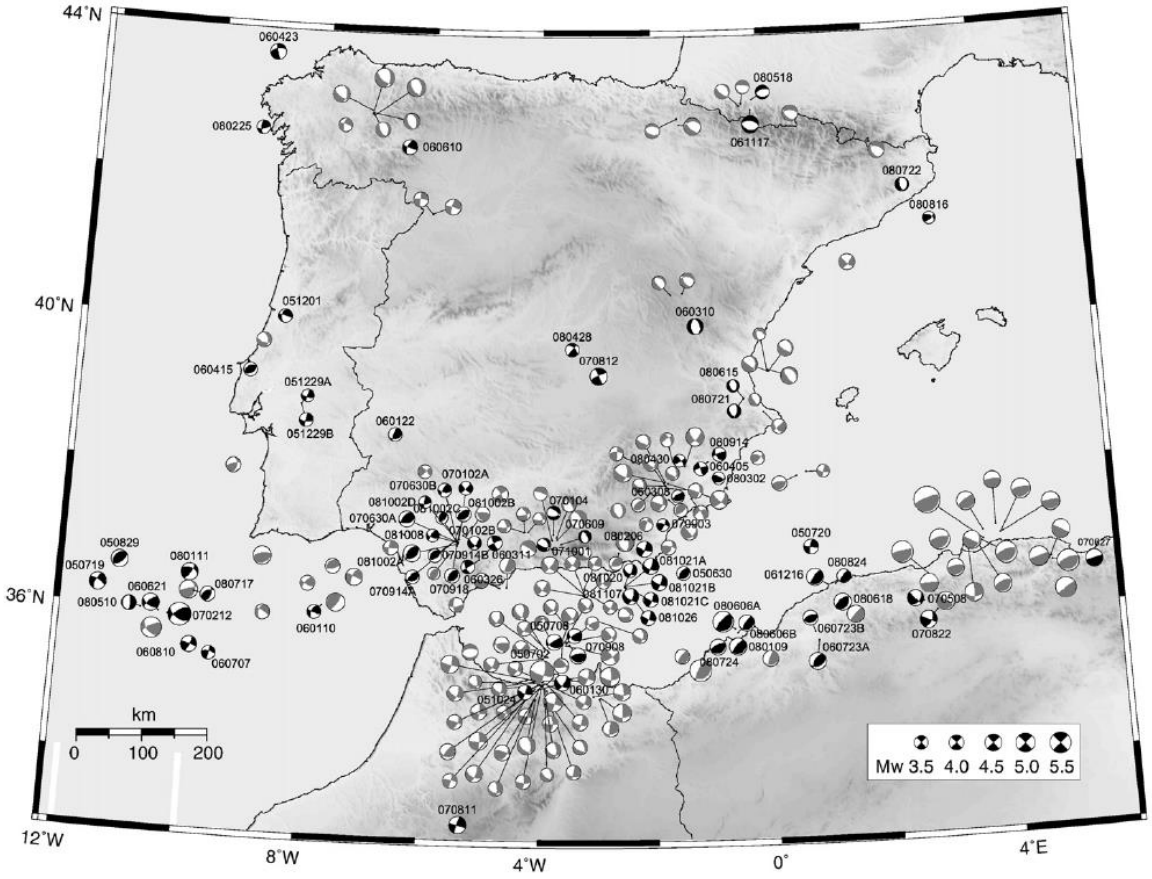

Figure 3: Focal mechanisms derived by Stich (2010) from solutions of the moment tensors for earthquake occurred during 2005-2008 time-span. (Stich et al. 2010)

The most recent and relevant study has been carried out by Palano et al. (2015), who analyzed 331 stations and compiled 56 additional vectors from other studies (e.g. Echeverria et al. 2013).

However, GPS has been widely used for measuring horizontal deformations the use of the vertical GPS deformation constitutes a difficult procedure. The precision of vertical positions is about 3–5 times lower than for the horizontal and many errors have to be modeled. Only two studies until now have presented vertical deformation rates of the CGPS stations of the peninsula: Serpelloni et al. (2013) and Nguyen et al. (2016). Serpelloni et al. (2013) presented the first contemporary vertical ground velocities in the Euro-Mediterranean region including 114 stations scattered throughout the Iberian Peninsula covering the central and southeastern regions. Nguyen et al. (2016), included 27 stations concentrated in the Pyrenees.

4. Methods

In this chapter we describe the input data and the procedures followed during the processing with the purpose of calculating the 3D velocity field of the Iberian Peninsula. We start by providing a brief introduction to GPS system to understand its basic characteristics.

4.1 Introduction to GPS system

GPS (Global Positioning System) is the most widely used GNSS (Global Navigation Satellite System) in the world. This system is based on the principle of trilateration, the method of determining position by measuring distances to points of known positions which provides 24-hour three-dimensional position, velocity, and time information to suitably equipped users anywhere on, or near, the surface of the earth (Hofmann-Wellenhof et al. 2008). It consists of three segments (Figure 4):

a) Space segment. Present day it is composed by 31 GPS operational satellites (https://www.gps.gov/). The orbit period of each satellite is approximately 12 hours, so this provides a GPS receiver with at least six satellites in view from any point on Earth, under open-sky conditions.

b) Control segment. It consists of a system of tracking stations located around the world which are responsible for the monitoring and operation of the space segment (Jeffrey 2010). The current Operational Control Segment (OCS) includes a master control station in Colorado Spring, an alternate master control station, 11 command and control antennas, and 16 monitoring sites throughout the world (https://www.gps.gov/).
c) User segment. Is the equipment (antenna, receiver and processing software) which processes the received signal from the satellites for positioning, navigation and timing applications.

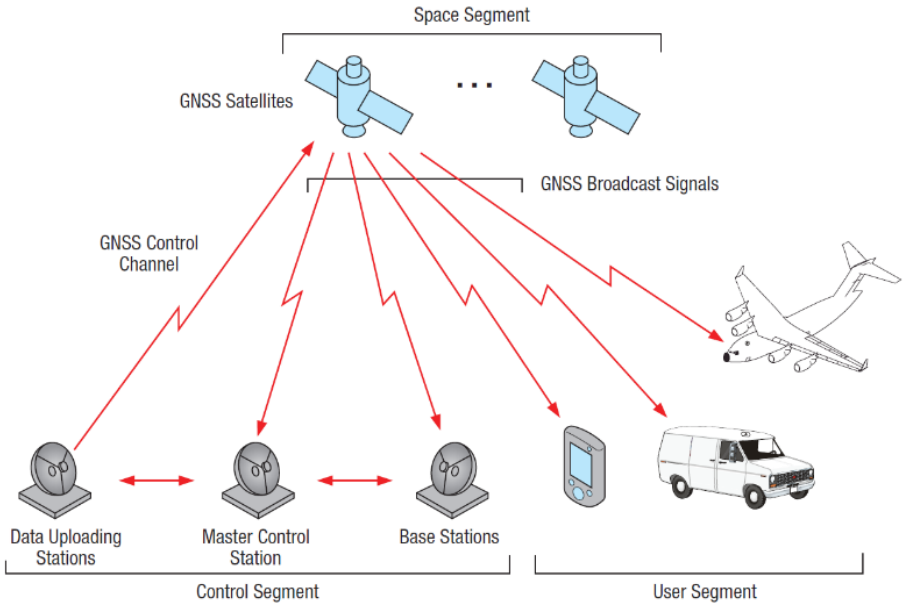

Figure 4: GNSS segments. (Jeffrey 2010)

There are several strategies that can be employed to determinate the coordinates of a single point when processing GPS data depending on the number of receivers used. *Point positioning* when using one receiver or *Relative positioning* when using more than two receivers and combining the data received from the same satellites (Blewitt 1997). In the present work the employed observation technique is static relative positioning, the most accurate method.

In relative positioning the coordinates of an unknown point are determined with respect to a known point (Blewitt 1997).This technique determinates the vector between the two points. A scheme of this technique is shown in Figure 5: assuming simultaneous observations at the know point (A) and the unknown point (B) to satellites j and k, linear combinations can be created from single-differences, double-differences and triple-differences (Blewitt 1997). Differences can be accomplished across receivers, satellites or time (Blewitt 1997).

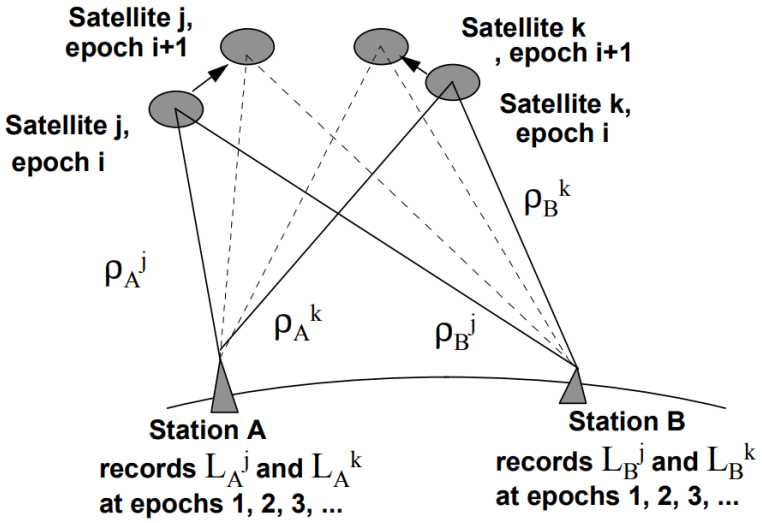

Figure 5: Relative positioning geometry from triple differences. (Blewitt 1997)

It has to be taken into account that there are some errors affecting GPS solutions. However, correcting files and parameters can be added and modelled when processing GPS data in order to correct some of these errors. This can be classified into four groups (Jeffrey 2010):

1) *Satellite related errors:* deviations from the satellite clock and orbital variations.
2) *Signal propagation related errors:* ionospheric and tropospheric delays due to refraction of the signal. The GPS signal cross the ionosphere and troposphere causing a change in the speed and direction of signal propagation.
3) *Receiver related errors:* deviations from the antenna clock, multipath of the signal before arrive at the antenna target and variations in the antenna phase center.
4) *Non-GPS related errors:* Errors related with the Earth surface deformation such as solid Earth tide, atmosphere and hydrological loading, and ocean and pole tide.

4.2 GPS data compilation

In this given work we use data coming from a continuously recording GPS stations (CGPS) scattered throughout the Iberian Peninsula, south of France and northern Africa (Figure 6). These stations are monuments containing a GPS receiver and antenna. The antenna remains permanently fixed at a point and raw observational data is stored continuously on the receiver and later made available on the internet to general public. The majority of the CGPS stations present in the Iberian Peninsula were installed for topographic applications, such as surveying and cadaster maps. Most of them are installed on top of the buildings and are prone to acquire lower-quality data, since they record not only the tectonic movements, but also the movements of the buildings and the monuments itself. Few existing network, such as CatNet in Catalonia or Topo-Iberia are designed to with more stable monuments suitable for tectonic studies. The used stations belong to a total of 22 regional GPS networks (Figure 6). With the exception of Topo-Iberia and UB network all CGPS data were retrieved from public repositories available in Internet. A description of these networks is provided in the appendix.

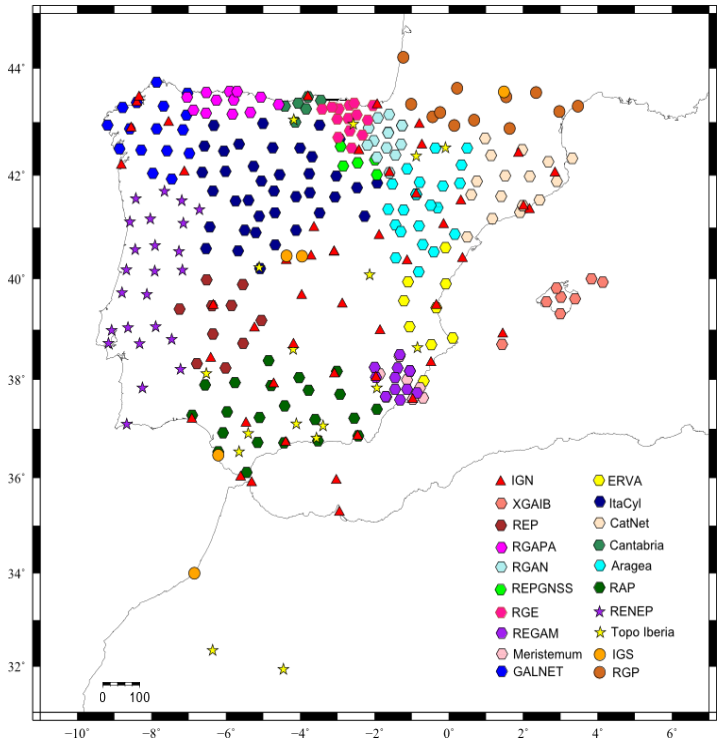

Figure 6: Distribution of the continuous GPS stations used in this study. The symbols of the stations are according to the belonging network.

For every station and every day in 2015-18 we obtained a raw data in the RINEX format, usually 2 to 3 Mbytes in size. Taking into account that we are processing a time-span of 2015.0 to 2018.3 for 405 stations, the amount of downloaded data to process is large (>450 000 RINEX files). In order to optimize the process and to fully take advantage of the 40 processors that the employed workstation possesses, we subdivide the stations into 13 subnetworks, with a maximum of 40 stations in each. Each subnetwork included the same 13 core stations (Figure 7), necessary for posterior combination of the subnetwork

solutions into a common reference frame. The process of the data compilation has resulted very laborious and time-consuming, since apart from the time that it takes to ftp data via internet some other problems occur. For example, due to the naming of the stations or the format off the original data. Every station has an ID composed of four characters (e.g. GATA for the UB station at Cabo de Gata). If two stations have the same 4-char ID, then the GAMIT software can obtain an erroneous apriori position for the station and the processing can fail. To avoid this conflict, we have renamed numerous stations with a new 4-char ID, making sure that the new name was not in conflict with some other stations. This was done using a SOPAC (http://sopac.ucsd.edu/) online tool.

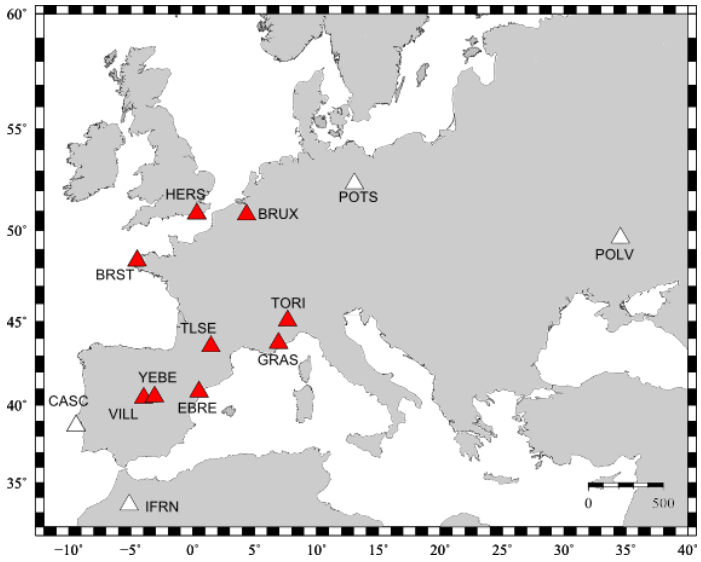

Figure 7: Core stations defined in this study. Stations are common in all the generated subnetworks. Stations shown in red were used for defining Eurasia fixed reference frame.

Other time-consuming procedure is related to the problems associated with the sampling rate of the available RINEX files. The input file in our study is a daily RINEX file with a 30-sec sampling. However, several networks (e.g. RENEP of Portugal) only provide hourly files with a 1-sec sampling, that have to be spliced tougher and down sampled to 30-sec. To optimize this process of re-formatting data we designed a suite of C-shell scripts based on the TEQC program (Estey et al. 1999).

4.3 GPS data processing

Once we had got the data, the analysis is performed using GAMIT/GLOBK software (Herring et al. 2008) from the MIT that uses double differences of the phase and code data on the ionosphere-free LC combination to compute a network solution (McClusky et al. 2003). GAMIT, process the raw GPS data (RINEX files) resulting in daily solutions. GLOBK, combines the obtained daily solutions given by GAMIT and generates position time-series and velocity fields.

We processed 3.3 years of data (2015.0 to 2018.3) from 405 recording CGPS stations described before. This time-span is sufficient to appropriately model the annual oscillations in the resulting time-series and achieve optimal resolution of the velocity solutions (Figure 8) (Blewitt and Lavallée 2002). The choice of this time-span is dictated by the limited time availability to complete this thesis, since the time of data processing increases with the amount of data analyzed as mentioned before.

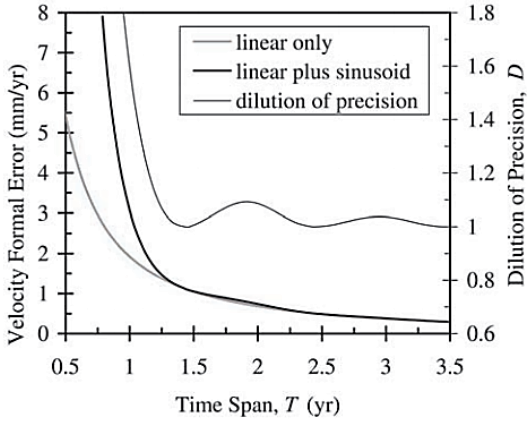

Figure 8: Velocity formal error (mm/yr) versus data span. No trend should be derived from results covering a time-span shorter than 2.5 years because the estimated motion can be significantly biased by seasonal variations and other signals. (Blewitt and Lavallé 2002)

To obtain GPS station velocities we have followed a three-step approach described by McClusky et al. (2003) and Echeverria (2015) as we show in Figure 9.

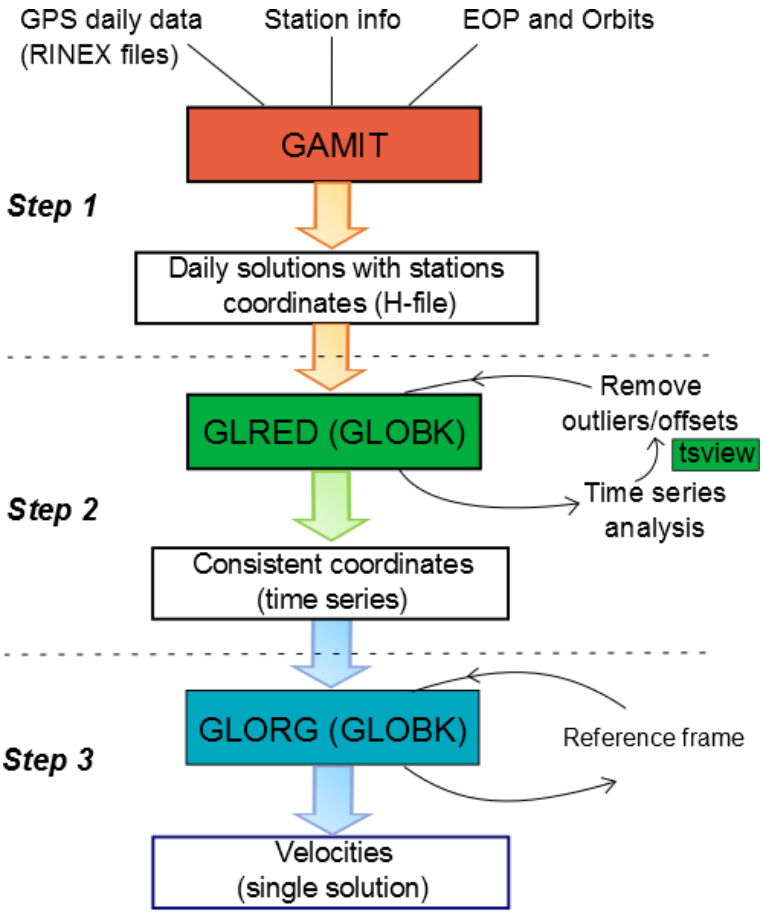

Figure 9: Summary scheme of the GPS data analysis using GAMIT/GLOBK software. It is represented the three-step approach proposed by McClusky et al. (2003) and Echeverria (2015).

Step 1 consists of processing daily GPS phase observations using GAMIT by applying loose a priori constraints (in order to estimate station coordinates), the zenith delay of the atmosphere at each station and orbital and Earth orientation parameters (EOP). It is called loose because all the estimated parameters at this step are estimated simultaneously without applying tights constraints. Each subnetwork need also the station info file which groups the information of the type of GPS receiver and antenna of each station. Also, and most important it has to include the changes of this devices that have been occurred during the time. If this information isn't accurate then it can derive in a source of error.

As a result, at this initial step we obtain a daily full covariance matrix (H-file) for each day and subnetwork computed with loose constraints on all parameters. This step is the most time consuming since a daily processing of only one subnetwork takes approximately 50 minutes. Thus, to process 13 subnetworks for 3.3 years would take more than 600 days on a machine with only one processor. Luckily, since we can run many processing jobs in parallel, taking advantage of the 40 cores of the available workstation at the UB, we can reduce this time to two months, approximately.

The **step 2** uses GLOBK module which enables us to calculate consistent station coordinate time-series in ITRF2014 reference frame from the loosely constrained daily solutions obtained in the previous step using GAMIT.

ITRF is the international reference system most used in geodynamic studies. This system is materialized by different stations spread around the world. It assumes that the entire Earth surface is moving (without any fixed plate) and that the velocities of all the stations sum up to zero (Altamimi et al. 2016).

The step 2 is iterative. The obtained raw time-series need to be analyzed in order to detect errors originated by position inaccuracies and offsets due to earthquakes, hardware or antenna changes. This is performed using tsview tools (Herring 2003) developed for Matlab. We applied a filter to remove obvious outlier points that exceeded 5 sigma values after de-trending the data, as well as the points that had uncertainties in their positions greater than 20 mm. Also we account for temporally correlated noise by using the first-order Gauss–Markov extrapolation (FOGMEX) algorithm proposed by Herring (2003) to determine a random-walk noise term, which we then incorporated into the Kalman filter used to estimate the velocities. The result of this filters can be views in a filtered time-series presented in Figure 10. To generalize, we can say that there are three main type of errors:

a) Outliers: points not coinciding with the average trending of all the data. Can be easily removed.
b) Gaps: data missing. Cannot be fixed, but you can use a longer time span to compensate for the missing data.
c) Offsets due to antenna or receiver changes. Can be fixed in tsview dividing the time-series in segments.

Once the errors are removed, it can be considered that the individual daily positions in all components are of a suitable quality and one can proceed to the next step of post-processing, to obtain a precise velocity of each station in the reference frame of ITRF2014 (Altamimi et al. 2016). However, we had to exclude some stations because either the time span was not long enough (since it was installed in 2016 or 2017) to reduce the velocity formal error (Figure 8) or the station presented errors during the processing step 1 and could not be fixed. Hence, we exclude them to avoid the contamination of the other results.

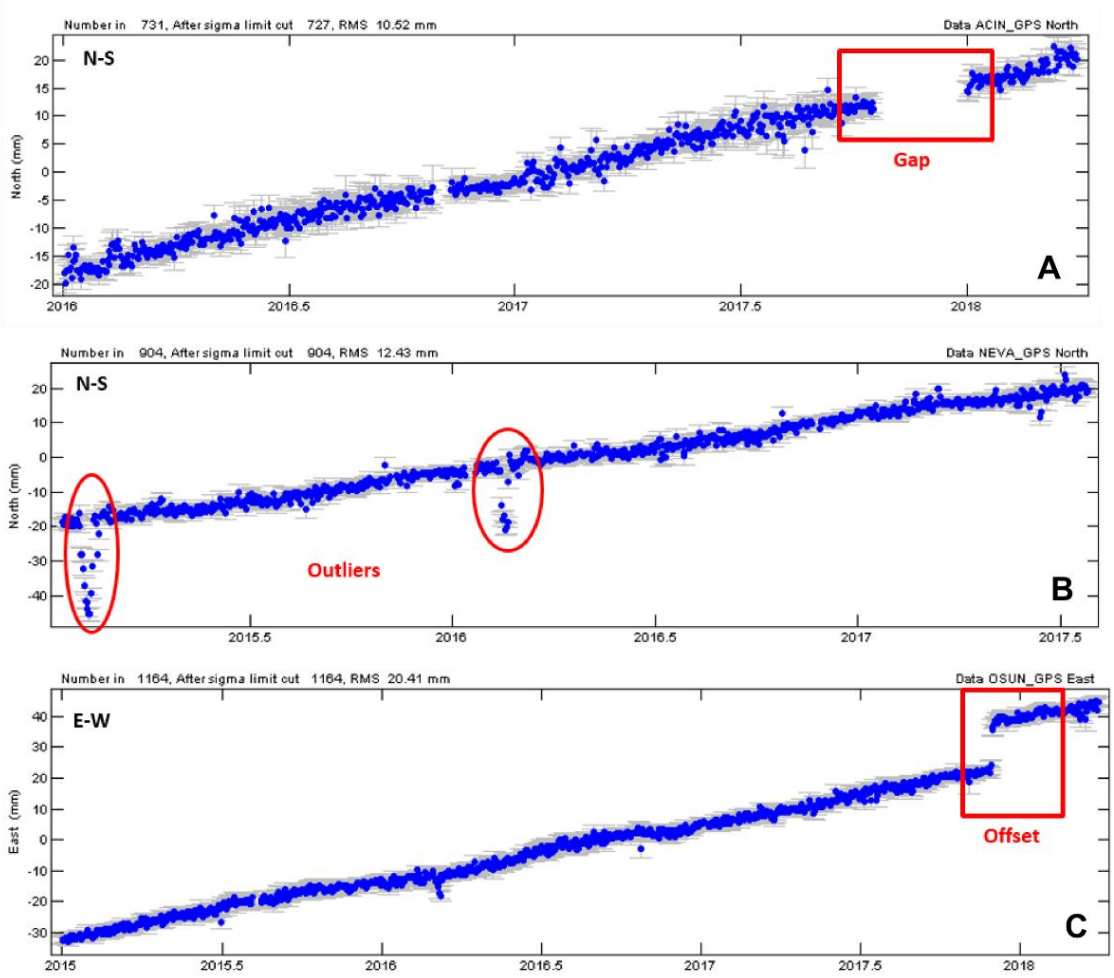

Figure 10: Typical errors in time-series: a) Gaps due to a lack of data (time-serie of ACIN station), b) Outliers (time-serie of NEVA station) in this case originated by freezing of the antenna during winter time in Sierra Nevada (where the station is located), and c) Offsets as a consequence of hardware or antenna changes and/or earthquake occurrence (time-serie of OSUN station). Time-series are in global ITRF2014 system (Altamimi et al. 2016).

The **step 3** consists in the estimation of the positions, velocities and uncertainties for each station in a Eurasia fixed reference frame, which is achieved by fixing a set of CGPS stations located on the stable part of Eurasia (that are part of the core stations). In our case, the following stations were used to define this frame: BRST, BRUX, EBRE, GRAS, HERS, TLSE, TORI, VILL, YEBE (Figure 7). Also, we overlapped our results with the obtained by Palano et al. (2015) and Serpelloni et al. (2013) to check the accuracy of the results.

4.4 Strain rate calculation

Strain rate parameters (extension, shortening, dilatation and shear stress) were calculated from the computed horizontal velocities for each of the processed GPS station. The strain rate field calculation was performed using the SSPX software package (Cardozo and Allmendinger, 2009). This software calculates best-fitting strain tensors (using the inverse problem) given velocity vectors by using the next matrix equation (Cardozo and Allmendinger 2009; Echeverria 2015):

$$d = G * m$$

Being *d* the vector with known velocities, *G* the matrix with initial positions of the computed stations and *m* the vector of unknown model parameters. The software uses several strategies for calculating strain across a region (Cardozo and Allmendinger, 2009). These include: delaunay triangulation, grid-nearest neighbor and grid-distance weighted methods. We used the grid-nearest neighbor approach that computes strain rate at the center of each grid, with a grid spacing of 50x50 km and taking into account the 20 nearest stations located within a maximum distance of 200 km. These parameters provide a smoothed regional pattern, and some local strain field variations could have been missed.

5. Results

5.1 Velocity field

The main result of this work is the present-day 3D crustal deformation velocities presented in two different maps: one for the horizontal component (Figure 11) and one for the vertical component (Figure 13). A table with each velocity component is presented in the appendix with the respective errors.

5.1.1 Horizontal velocity field

In general, as expected, the calculated deformation rates are low since the convergence rate between Eurasia and Nubia plates ranges between 4.5 and 5.6 mm/yr (DeMets et al. 1994; Argus et al. 2011). The highest velocities occur next to Gibraltar where the plate boundary between Nubia and Iberia passes. The lowest velocities are found in the Pyrenees and the central part of the Iberian Peninsula. Different generalized patterns of motion can be identified from the 2D velocity field shown in Figure 11, where Eurasia-fixed reference frame is used.

The southern part (domain 1) move with 4-5 mm/yr rate in WNW-NW direction, roughly parallel to Nubia/Iberia convergence. Just northward, further away from the plate boundary, domain 2, shows a reduction of the velocities to ~2 mm/yr. In this domain the direction tends from WNW to NWN. Towards the east, in the Eastern Betic Shear Zone, another domain can be identified (domain 3), with a distinctly different sense of motion, where the velocities trend northward (NW to N) with rates ranging from 0.5 to 2 mm/yr. In contrast, domain 4 to the north, moves mainly in a SE direction (opposite to the convergence of Nubia and Iberia) with rates below 2 mm/yr. Domain 5 includes the northwestern area of the Iberian Peninsula where velocities trends to NE with low rates (comparing to the other domains) below 1 mm/yr. This direction changes from NE to more N in the Basque country and French Pyrenees constituting domain 6, where the rates are as low as in domain 5. The easternmost region (domain 7), comprising of Catalonia, the Catalan Pyrenees and the Balearic Islands, shows a direction from E to NE, with rates increasing towards the Balearic Islands from nearly zero to 3 mm/yr.

Some stations show an anomalous behavior, in their direction or the magnitude or both. We consider that a value higher than 2 mm/yr for the stations located away from the plate boundary cannot represent a tectonic motion. As mentioned earlier, the analyzed stations comprise of different monument types, and

their long-term stability is questionable. The dominant monument type is a steel mast anchored to a building. Few monuments are directly anchored to the bedrock. Hence, the observed geodetic monument instability is due to varying conditions of the anchoring media coupled with local processes. This anomalous behavior could be mainly related to the monument instability of the stations and/or buildings, but there are cases when anomalous motion (stations LORC and LRCA in Guadalentín basin, Lorca), where its motion is real, but caused by the terrain subsidence (González et al. 2012; Frontera et al. 2012; Tagliaferro 2017).

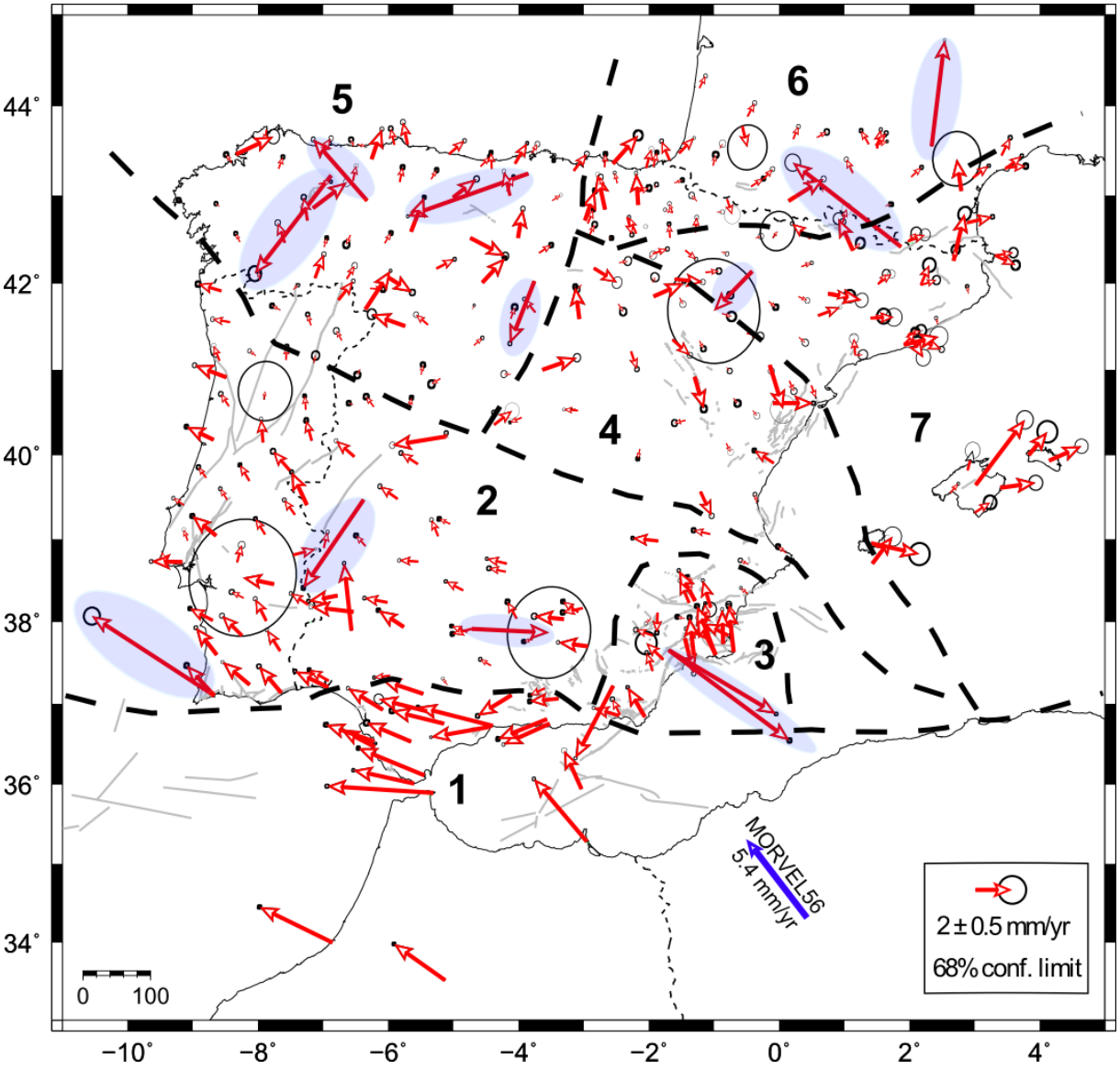

Figure 11: Map of the 2D GPS velocity field of the Iberian Peninsula in a Eurasia fixed reference frame with the interpreted velocity domains. Velocity vectors are in a 1 scale value and 68% of confidence. The confidence interval is represented as a circle at the arrowheads and shows the margin of error of the data. Anomalous velocities are highlighted in blue. Blue vector indicate the MORVEL 56 convergence of Africa and Eurasia (Argus et al. 2011). Dashed black lines delimits national borders. Grey lines represent faults that have been active during the Quaternary period (retrieved from QAFI database).

Interestingly, perhaps not too obvious, but still important correlation can be identified between the seven velocity domains defined in this study and the geo-tectonic configuration of the Iberian Peninsula (Figure 12). The SW part of the Iberian Peninsula moves in the same direction as North Africa (e.g. Nubia plate), suggesting that the domain 1 is more likely to belong to the Nubia plate. Meanwhile, domain 2 located on top of domain 1, coincides with the southern part of the Iberian Massif. The regional configuration of the Eastern Betic Cordillera (the EBSZ) is complex and shows a distinct pattern of motion (domain 3). Above

it, domain 4 incorporates all the Iberian cordillera and its limit with domain 7 coincides with the limit between this cordillera and the Ebro basin. In addition, the limit between domain 6 and 7 in the northeastern part, coincides well with a geotectonic boundary between the Pyrenees and its foreland Ebro basin. The eastern boundary of domain 5 more or less coincides with the limit between the alpine cordilleras (Pyrenees and Iberian Cordillera) and the north part of the Iberian Massif. Additional, potentially important observation is related to the fact that in every domain, calculated velocities are perpendicular to the direction of the tectonic structures (Figure 12A), perhaps with the exception of the Balearic Islands. This suggests that the previous structures facilitate the actual strain configuration.

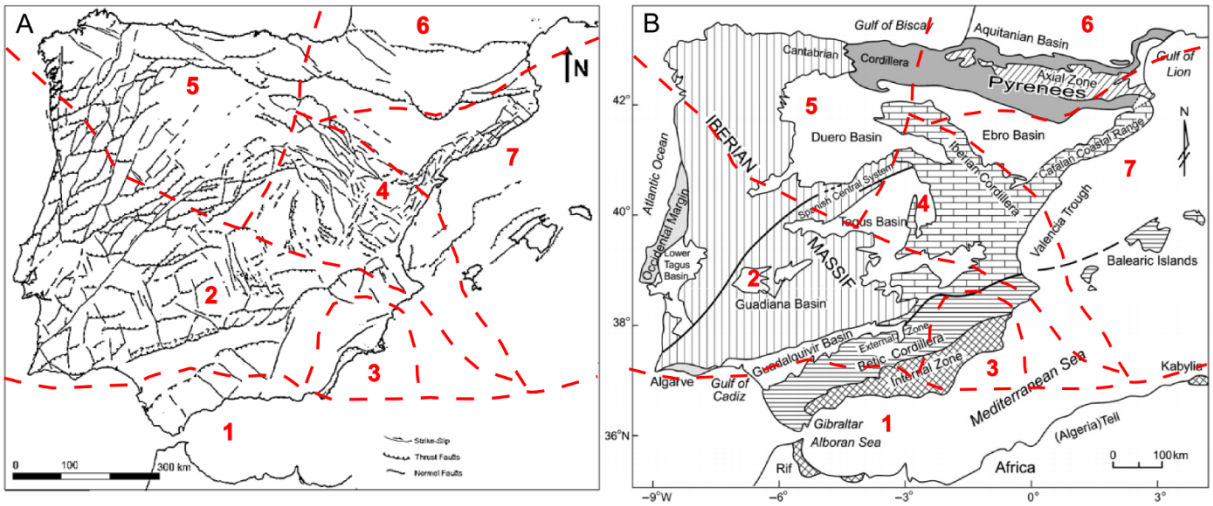

Figure 12: Comparison of the domains derived by the obtained velocity field with the structural configuration of the Iberian Peninsula. Map from A) (Vera 2004) B) (Badal et al. 2011; Sanz de Galdeano 2000)

5.1.2 Vertical velocity field

First of all, it should be underlined, that the presented vertical velocity field is preliminary and is most likely to be changed in the future with a more in-depth data processing. In the presented map of preliminary vertical motions (Figure 13) a distinct pattern of uplift and subsidence can be identified in two areas: while the NE of the Iberian Peninsula is subsiding, the SW part is undergoing uplift. The majority of rates range from -4 to 4 mm/yr. Some points showing high rates are related to local processes triggered by anthropogenic activities. For example, in the SE, located in the town of Lorca there is a station (LRCA) showing a rate of -66 mm/yr. This rate is not anomalous since this region is affected by a high subsidence due to the groundwater withdrawal of the aquifer of Alto Guadalentín for agriculture and urban use (Rigo et al. 2013).

Although, we have introduced models to remove factors affecting the vertical GPS signal such as, ocean loading and ocean tides, it is possible that the obtained results are contaminated by an erroneous choice of the reference frame, resulting in a long wavelength tilt with an axis-oriented N-NW to S-SE passing roughly in the middle of the peninsula (B. King, pers. comm.). Additional errors can be related to the unmodeled effects of glacial isostatic rebound and atmospheric delays.

5.2 Geodetic strain rate

From the GPS velocity field we could obtain the strain-rate field using SSPX software (Cardozo and Allmendinger 2009) as mentioned in the previous chapter. This series of maps (Figure 14) allow us to identify regions with the highest deformation rates and relate them with the known seismic faults and earthquakes. Not surprisingly, the maximum deformation signal is observed in the EBSZ and northern Alboran Sea, seismically the most active regions in the peninsula (Figure 2).

Extension and shortening (Figure 14A and 14B)

Extension is represented in red while shortening in blue. Maximum extension can be observed in the Pyrenees region and in the central-external Betics. These results are well correlated with the focal

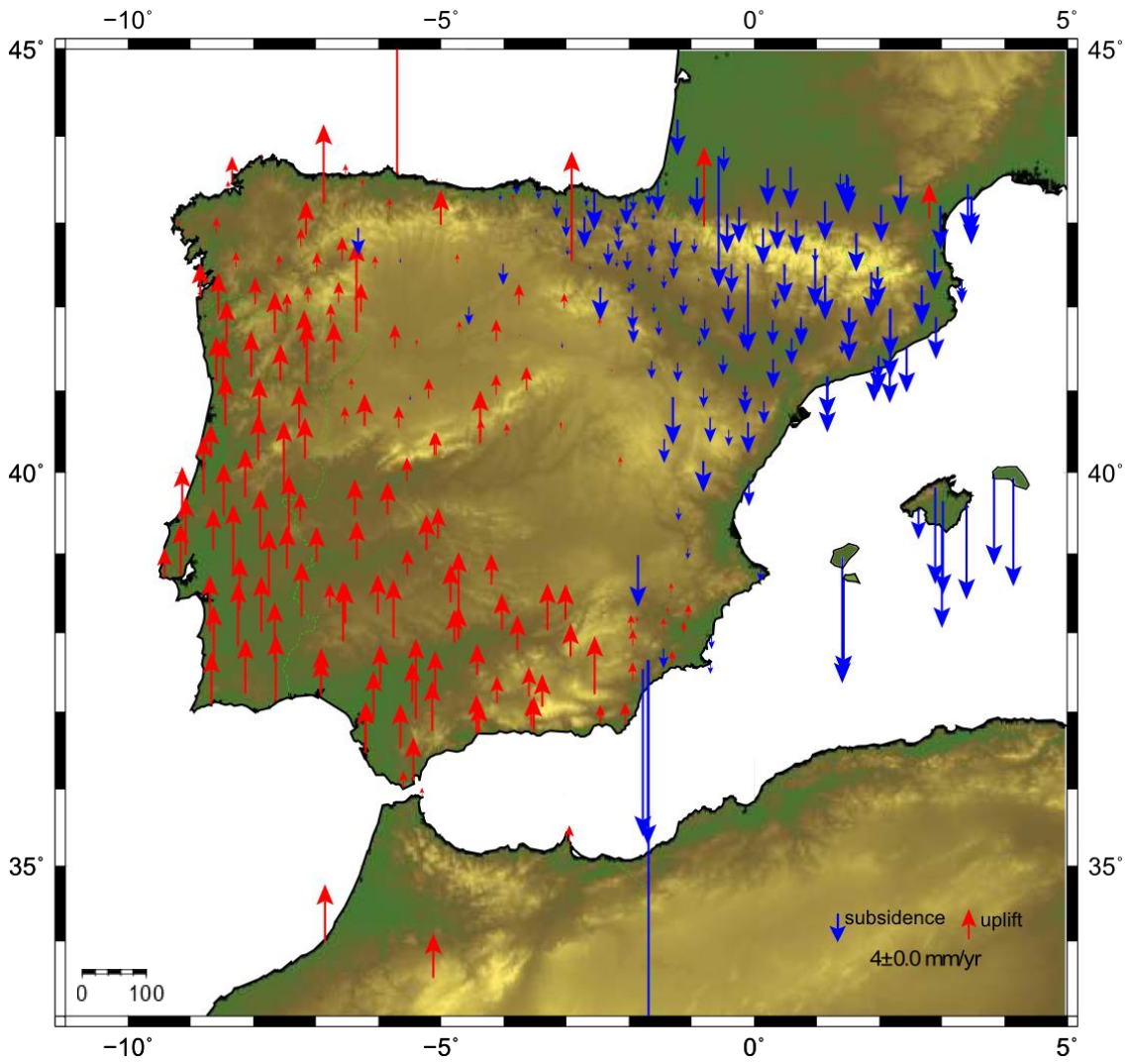

Figure 13: Map of the GPS vertical velocity field over the Iberian Peninsula. Red and blue arrows show uplift and subsidence, respectively.

mechanisms (Figure 3) which show dip-slip normal faulting and a direction N-S for the tensional stresses in the Pyrenees and ENE–WSW in the central-external Betics. Maximum shortening occurs in the Alboran Sea and the Eastern Betic Shear Zone (Figure 14B). Correlation with focal mechanisms is also coherent. The Algerian part of Africa margin and the Alboran sea show reverse type focal mechanisms due to shortening between Nubia and Iberia tectonic plates with an NW-SE direction. For the EBSZ, shortening is most likely driven by the same force, and is expressed as a minor compressive component observed in the Alhama de Murcia (e.g. Martínez-Díaz and Hernández-Enrile 1992; Masana et al. 2004) and/or Carboneras faults (e.g. Moreno 2011; Echeverria 2015) and 2011 Lorca earthquake focal mechanism (Martínez-Díaz et al. 2012).

Maximum shear strain (Figure 14C)

According to our strain rate calculation the maximum shear strain occurs in the EBSZ and Alboran Sea and wanes in the rest of the Peninsula. In the EBSZ focal mechanisms are predominantly left-lateral strike-slip with NNW-SSE shortening direction. We can observe that within the Betic Cordillera faulting style changes from predominately strike-slip in the EBSZ towards predominately normal faulting in the central-external Betics.

Dilatation (Figure 14D)

A negative value of dilatation rate (blue) indicates an excess of shortening in the horizontal plane and requires vertical thickening to maintain constant volume. On the contrary, when the dilatation is positive

(red), there is an excess of extension and vertical thinning is required to maintain constant volume (Cardozo and Allmendinger 2009).

Negative dilatation occurs in the EBSZ and Alboran Sea since it is the structure which absorbs much of the deformation between Nubia and Iberia. Moreover, it occurs in the offshore of Galicia and Asturias (NW of Iberian Peninsula) due to the transmission of the strain along the Iberian plate that also generates seismic activity in the NW (López-Fernández et al. 2008). Herraiz et al. (2000) state a general shortening in this area with a NW-SE direction. Positive dilatation occurs in the Pyrenees and in the Iberian Massif. One hypothesis of the extension occurring in these areas is that is caused by an isostatic rebound due to the uplift and erosion of the cordilleras (Asensio et al. 2012; Vernant et al. 2013).

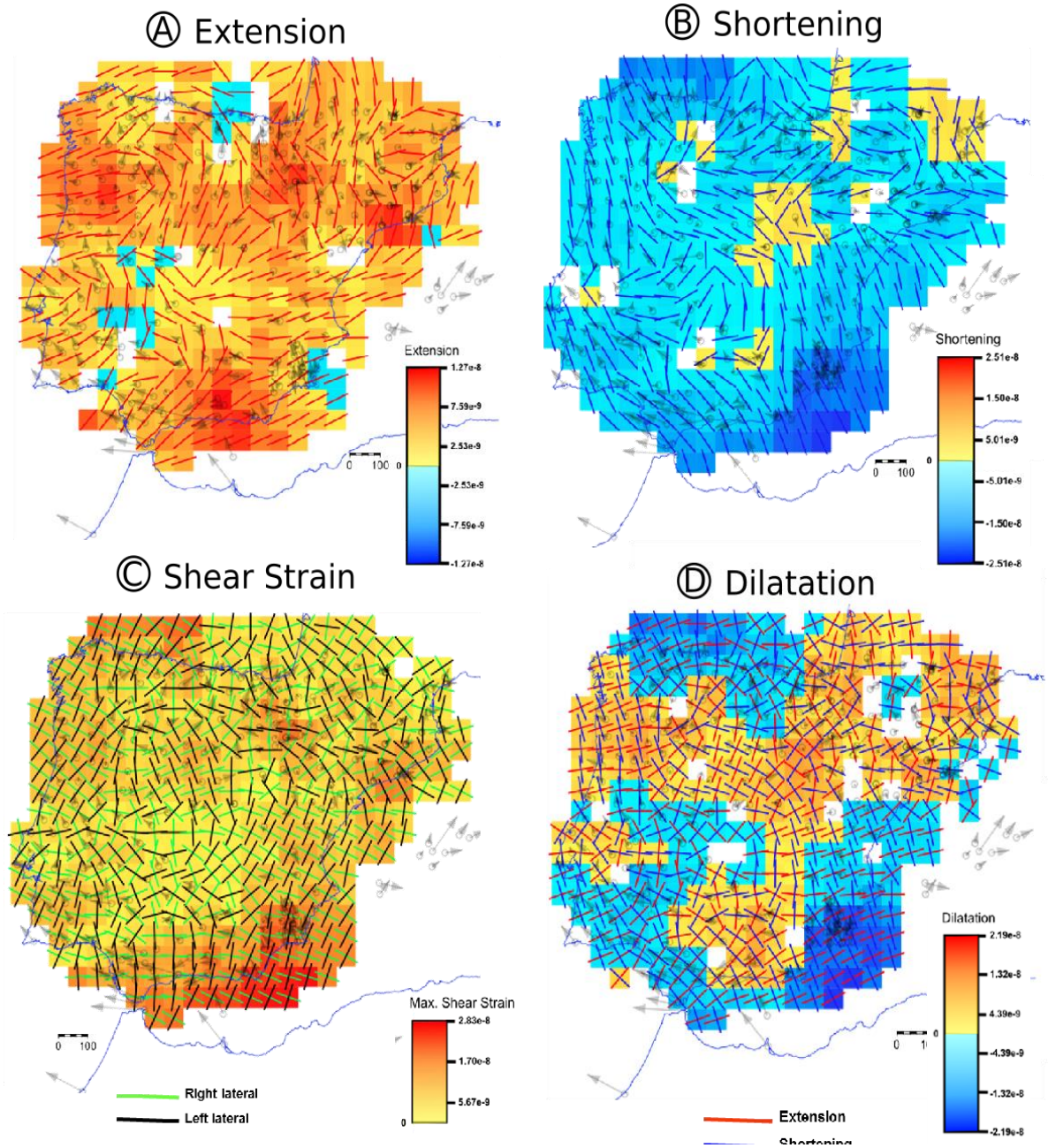

Figure 14: GPS strain rate field computed for the Iberian Peninsula showing the strain rate axes. A) Extension B) Shortening C) Maximum shear strain rates. D) 2D dilatation strain rates.

6. Discussion

In the following chapter we discuss the main findings of the presented work. First, we compare the obtained results with previous studies to check the quality and reliability of the presented results.

Afterwards, we illustrate the usefulness and the applicability of the obtained results in the calculation of regional seismic hazard assessment maps.

6.1 Comparison with other studies

For the horizontal component of motion we compared our velocity field with the results of Palano et al. (2015), since it is the most recent relevant study carried out in our study area. In general, without taking into account anomalous velocities of individual stations, both of the velocity fields are coherent and very similar. There is just a slight difference in orientation of the velocity vectors (Figure 15), most likely caused by the use of different Eurasian plate fixed reference frame. Palano et al. (2015) has suggested a large-scale clockwise rotation of the southern and the western sectors of the Iberian Peninsula. To test this hypotheses they estimated the Euler vector components for the Iberian block and determined a clockwise rotation rate of 0.07 deg/Myear. Our velocities also show this pattern of rotation, which can be seen in the motion of the domains 2, 4 and 5 (Figure 11), reinforcing the observation of Palano et al. (2015). However, more in-depth study of this rotational phenomenon, including inversion and block modeling (Khazaradze et al. 2014b) was out-of-scope of the conducted work, and will have to be addressed in the future.

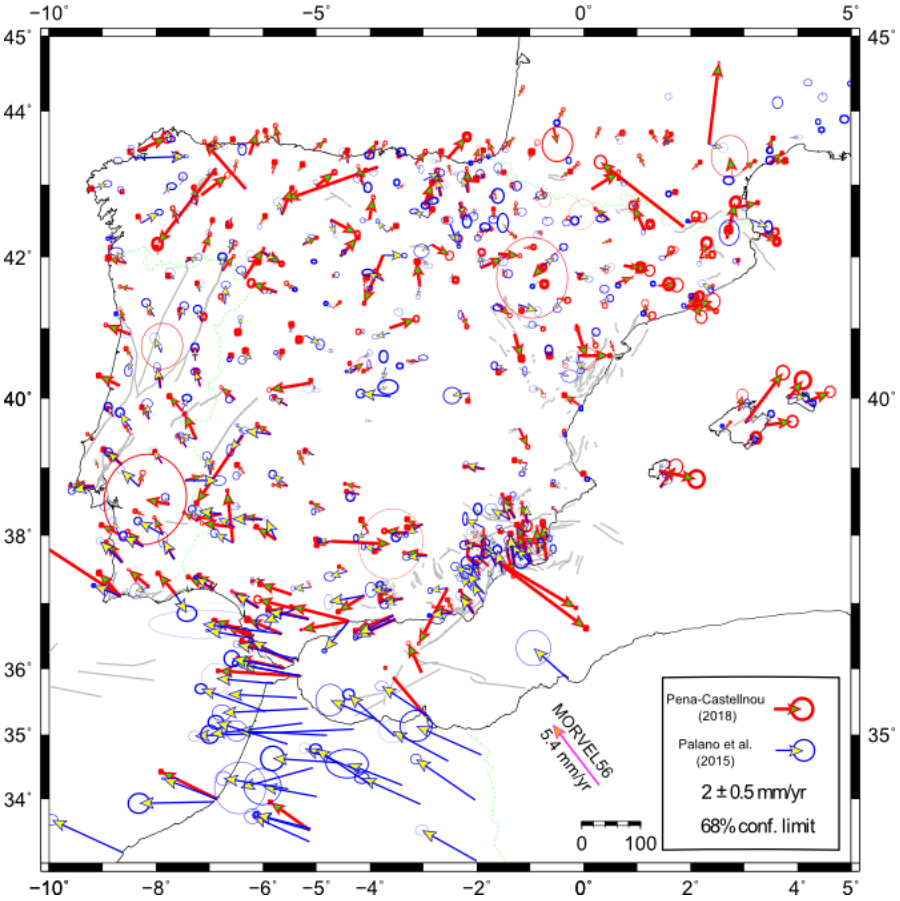

Figure 15: Comparison of the horizontal velocity field derived in this study (red arrows) with the results of Palano et al. (2015) (blue arrows). Velocity vectors are in a 1 scale value and 68% of confidence. The confidence interval is represented as a circle at the arrowheads and shows the margin of error of the data. Pink vector indicate the MORVEL 56 convergence of Africa and Eurasia (Argus et al. 2011). Grey lines represent faults that have been active during the Quaternary period (retrieved from QAFI database).

For the vertical component we compared our velocity field with the results of Serpelloni et al. (2013) (Figure 16). Their data show a dominant pattern of a regional subsidence with varying rates. Uplift is localized in central Iberia and in the southeastern part of Spain, but just few stations show these values. The results of Serpelloni et al. (2013) are obviously not correlated with our vertical motion results, which can be explained by the fact that our results, especially in terms of the vertical motions, remain to be preliminary and most likely contain some systematic errors.

While GPS method has been widely used for measuring horizontal deformations with high precisions, the use of vertical GPS deformation remains a challenge, and therefore very few studies use them (e.g. Bennett and Hreinsdóttir 2007). The two-or-three-fold lower precision of the GPS vertical component (with respect to horizontal) is related to tropospheric water vapor, unmodeled phase delays, mismodeled satellite orbital motions, variations in ground-based antenna phase centers, different loading processes, monument instability and the geometry of the satellite orbits (e.g. Blewitt and Lavallée 2002). For this reason, our data has to be considered as preliminary. Additional processing of the data from the previous years is needed, as well as more studies of reference frame definition and its stability in the vertical component.

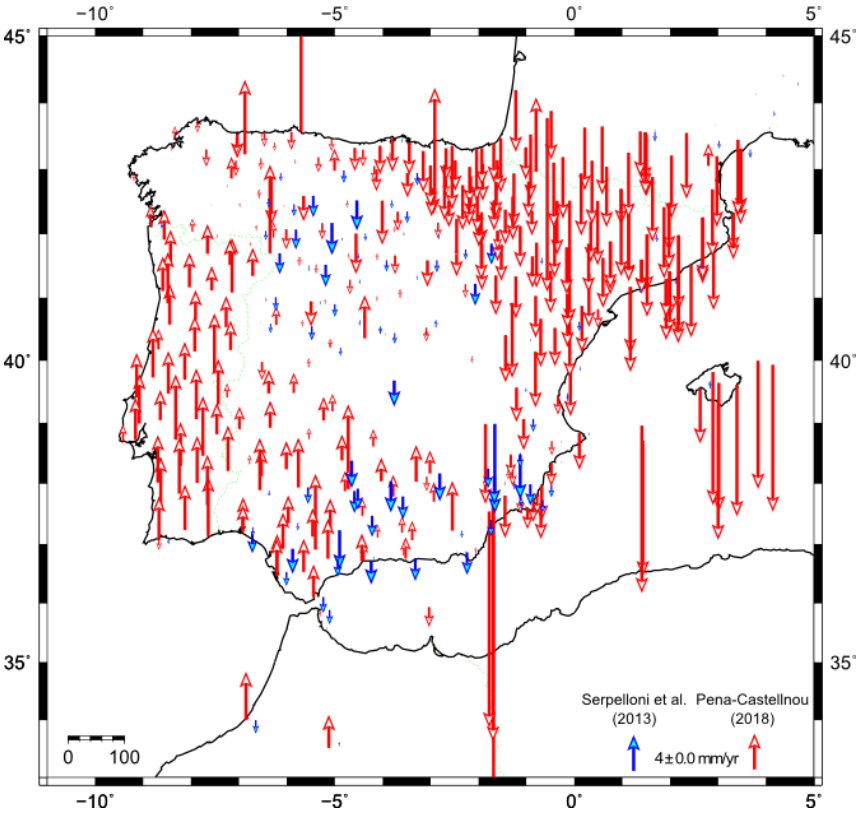

Figure 16: Comparison of the obtained results for the vertical component of the velocity field computed in this study (red arrows) with the results of Serpelloni et al. (2013) (blue arrows).

6.2 Applications for seismic hazard assessment

Seismic hazard analysis integrates geophysical, geological, and geodetic data to estimate earthquake potential. If the seismic properties of the faults can be analyzed benefiting from data with high spatial and temporal resolution, earthquake related losses can be significantly reduced (e.g. Ozener et al. 2009). GPS can provide observations of the gradual accumulation of tectonic strain along the faults before this strain is suddenly released as earthquakes which is one of the essential components in forecasting seismic hazards. This technique is especially convenient in areas with slow rates of deformation, like the Iberian Peninsula, in order to make long-term earthquake predictions more reliable.

In this study, as a result of obtaining a uniform 2D GPS velocity field, we were able to define distinct tectonic domains or blocks characterized by similar kinematic behavior. Also, as a result of the strain-rate field calculation, we identified regions with the highest deformation rates which are well related with the known seismic faults and earthquakes, specifically with the EBSZ and the Alboran Sea. It is well-known that these areas have the highest seismic hazard in the Iberian Peninsula. However, other areas, where relatively low GPS deformation rates are observed, should not be underestimated either, since they often present significant seismic activity and have been prone to the occurrence of several important historical earthquakes (e.g. 1428 Queralbs (Girona, EMS IX-X)). These areas include the Pyrenees, the northwestern part of the Iberian Peninsula and the south of Portugal.

GPS velocity field may contribute to define or adjust seismogenic zones for a better seismic hazard estimation. A seismogenic zone is a seismic source with homogenous seismic and tectonic characteristics formed by one or various seismic structures being a calculation method of the seismic hazard (Amaro-Mellado et al. 2017) . Several models of seismogenic zones were designed for the Iberian Peninsula: IBERFAULT, SHARE and COMISIÓN (García-Mayordomo 2015); present-day used in the Spanish Building Seismic Regulations. Nevertheless, these models do not include GPS strain rate measurements, since a decade ago the availability of this type data was poor and restricted at the southern part of the Peninsula and in the Pyrenees. At present, the calculated GPS strain rates by Palano et al. (2015) and in the present work may be an additional input data for the models of seismogenic zones.
In addition, the temporal study of the GPS strain rate accumulation could also be attempted, with the aim predicting future earthquakes by calculating the accumulated seismic energy since the occurrence of the last known earthquake (elapsed time of the inter-seismic period) (Ozener et al. 2009). This procedure is conceptually plausible, but the predictions performed might be affected by considerable uncertainty, since the connection between the level of strain and the probability of earthquakes is not too clear (Cenni et al. 2015). On the other hand, the calculated vertical velocity could be useful for seismic hazard assessment in faults where a vertical motion dominates (e.g. dip-slip reverse and normal faults), whereas horizontal velocity field is more useful in studying reverse faults where horizontal elative dominates. Additionally, the GPS deformation data is useful for multi-risk analysis since it can provide information of undergoing uplift/subsidence that can be originated by a tectonic source (faults), landslides, sediment settlement and anthropogenic activities (e.g. groundwater extraction, mining, etc.).

In the following sections of this chapter a description of chosen specific areas will be provided in terms of the seismic hazard framework.

6.2.1 Eastern Betic Shear Zone

The velocity field and strain rate calculated in this study provide clear evidence of present-day tectonic activity of the EBSZ implying continuing strain accumulation on regional faults. The EBSZ is composed of an active system of left-lateral strike-slip faults which absorb the deformation between the Nubia an Iberian tectonic plates. This area shows a distinctly different sense of motion, where the velocities trend northward (NW to N) with rates ranging from 0.5 to 2 mm/yr in agreement with the main thrusting regime inferred by geological features (Figure 17). Domain 1 moves with 4-5 mm/yr rate in WNW-NW direction, roughly parallel to Nubia/Iberia convergence. Just northward, domain 2, shows a reduction of the velocities to ~2 mm/yr, trending WNW to NWN.

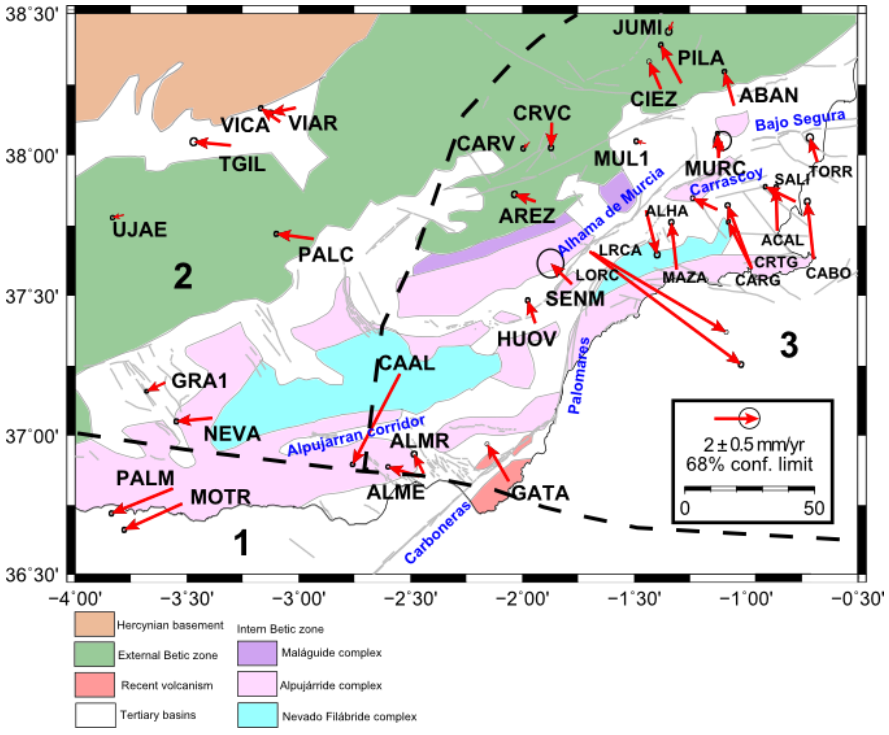

Figure 17: Easter Betic Shear Zone velocity field with the interpreted velocity domains. Velocity vectors are in a 1 scale value and 68% of confidence. The confidence interval is represented as a circle at the arrowheads and shows the margin of error of the data. Grey lines represent faults that have been active during the Quaternary period (retrieved from QAFI database).

Domain 1 and 2 show an opposite sense of kinematics compared with the domain 3. Palano et al. (2015) proposed a hypothesis to explain this change of motion: EBSZ may be related to an independent tectonic block which is trapped within the Nubia–Iberia collision, transferring a fraction of the convergence rate along the westernmost Algerian margin into the Eastern Betics. Regionally, Martínez-Díaz and Hernández-Enrile (2004) and Echeverria et al., (2015) proposed that the change of motion observed between Carboneras and Alpujarras faults (well-observed at stations PALM, MOTR, GATA and HUOV in Figure 17), facilitates a westward tectonic escape of the wedge bounded by the two strike-slip faults, favoring the formation or reactivation of NNW-SSW normal faults perpendicular to the east-west escape of the block (e.g. Giaconia et al. 2015).

During the last decade, numerous paleoseismological studies have been carried out in the EBSZ in order to obtain slip rates and other parameters of the faults. It is very useful to compare paleoseismological slip rates with the fault slip rates obtained with GPS. To obtain the GPS slip rate of a fault from a velocity field in a Eurasia fixed reference frame, several steps needed to be taken (Echeverria et al. 2015): 1) one station, located on the hanging wall of the fault, has to be fixed and then, 2) other velocity vectors, mainly located on the opposite foot wall of the fault, need to be projected into the fault plane. Since this type of detailed studies, targeting individual faults, were out-of-scope of the conducted work and the available period of time for the realization of this thesis was limited, this type of calculation has not been conducted.

6.2.2 South Portugal

We chose to examine this area due to its potential seismic risk. It is located in an area closer to the present-day plate boundary of Iberia and Nubia tectonic plates and presents an elevated seismic activity (Figures 2 and 3). Also the historical earthquake of 1755 (EMS 8.5) which devastated the city of Lisbon occurred in this area. The obtained velocity rates range from 1.3 to 2 mm/yr showing an N-NW direction (belonging to the proposed domain 2) (Figure 18). This area is problematic when doing a seismic hazard study due to the lack of Quaternary sediments. It is characterized by a strong coastal erosion exposing the Paleozoic basement and some Cenozoic and Mesozoic sediments (Figure 18). For this reason, GPS technique becomes important in order to determine slip rates of the faults.

Considering the proposed large-scale clockwise rotation of the southern and the western sectors of the Iberian Peninsula, Cabral et al. (2017) reported a possible change from reverse to strike slip motion of the faults in the area (e.g. São Marcos−Quarteira fault), possibly caused by the clockwise rotation. The seismic hazard of a fault is strictly dictated by its characteristics. If the behavior of the fault changes to a strike-slip type, the associated seismic hazard needs to be revised as well.

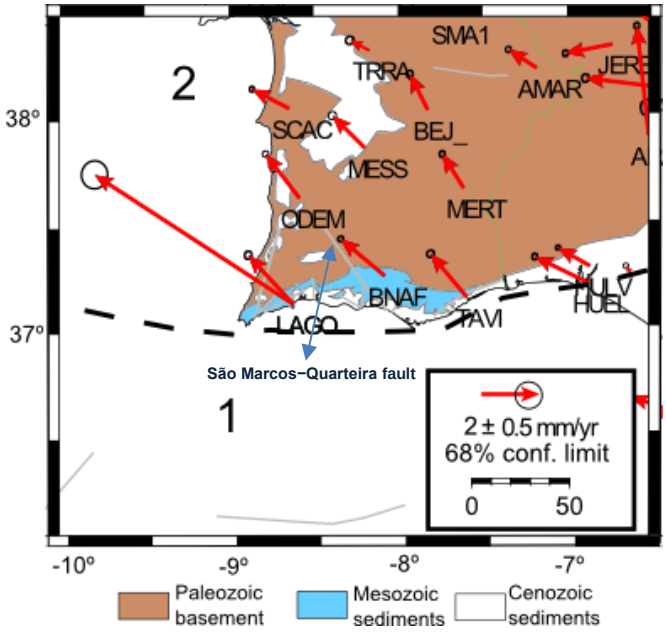

Figure 18: South Portugal velocity field with the interpreted velocity domains. Velocity vectors are in a 1 scale value and 68% of confidence. The confidence interval is represented as a circle at the arrowheads and shows the margin of error of the data. Grey lines represent faults that have been active during the Quaternary period (retrieved from QAFI database).

7. Conclusions and future research

The Iberian Peninsula is presently tectonically active and deforming. The calculated GPS velocities indicate that the Iberian Peninsula presents a heterogeneous velocity field which can be roughly grouped into 7 domains or blocks. Each domain is influenced by the structural configuration of the Iberian Peninsula and by the proximity to the Iberia-Nubia plate boundary. The highest rates (with respect to Eurasia) are found in the EBSZ and along the Iberia-Nubia plate boundary. The maximum velocity of 4.5 mm/yr, is observed at MELI station in Melilla. The lowest rates are located in the center of the Peninsula and along the northern margin reaching the Pyrenees. We consider that a value higher than 2 mm/yr for the stations located away from the plate boundary cannot represent a tectonic motion. Hence, some stations show an anomalous behavior which could be related to the monument instability of the stations and/or buildings. However, there are cases where the anomalous motion is caused by the terrain subsidence (stations LORC and LRCA in Guadalentín basin in Lorca).

From the obtained 2D GPS velocity field the strain-rate field of the Iberian Peninsula was calculated, which is well related with focal mechanisms derived by earthquakes. The highest deformation rates are observed in the EBSZ and northern Alboran Sea, seismically the most active regions in the peninsula. Shortening and shear strain occur mainly in this area, since it is where much of the shortening between Iberia and Nubia plates is concentrated. Another interesting phenomena is the positive dilatation that occurs in the Pyrenees and Iberian Massif. This extension is due to a isostatic rebound as a consequence of the uplift and erosion of the cordilleras (Asensio et al. 2012; Vernant et al. 2013).

The obtained data has applications in seismic hazard assessment. GPS can provide observations of the gradual accumulation of tectonic strain along faults before this strain is suddenly released as earthquakes. This technique is especially convenient in areas with slow rates of deformation, like the Iberian Peninsula, in order to make long-term earthquake predictions.

The obtained vertical velocity field has to be considered as a preliminary. The computation of the GPS vertical component is a new technique in needs further development, since many factors have to be taken into account. Although, in our processing we have introduced various models to remove some of the factors effecting the vertical signal, it seems that the obtained results are contaminated by an erroneous choice of the reference frame, resulting in a long wavelength tilt: where the NE of the Iberian Peninsula is subsiding and the SW part is uplifting. The majority of the vertical rates range from -4 to 4 mm/yr. However, there are some points showing high rates which are related to local processes triggered by anthropogenic activities (e.g. groundwater extraction, mining). This kind of data is useful for multi-risk analysis since it can provide information of ongoing uplift/subsidence that can be related to a tectonic source (faults), landslides, sediment settlement and anthropogenic activities (e.g. groundwater withdrawal, mining).

In order to better understand the kinematics of the study area and help to answer open questions not solved in this work, the future research should be addressed as it follows:

- Extend time-series backwards to 2010, mainly to resolve better the vertical signal.
- More care with the models in the GPS processing that might affect the vertical signal (ocean loading, tide loading, etc.).
- Compare the vertical velocity solutions with the sea-level change results, erosion rates, GIA, mountain building tectonic processes and anthropogenic processes.
- Compute GPS strain rates of seismogenic faults.

Acknowledgments

I would like to express my sincere gratitude to the supervisor of this thesis, Giorgi Khazaradze, for his continuous guidance and valuable reviews. The quality of this work would not be the same without his contributions.

I wish to thank the institutions responsible for the operation of the continuous GPS stations: IGN, EUREF, and IGS. Also, the autonomous communities of Spain for their effort in maintaining the geodetic networks and making the data freely available to the society, including the scientists.

To my colleagues (Carla, Anna, Albert F., “Mandi”, Martí, Miquel, David, Gemma, Diego, Nil, Filella,, Daniela), family, professors and all those who I have crossed during the unforgettable 5 years that I have been in the Faculty of Geology of the University of Barcelona learning what I like most. And to Carsten, for his support and love.

References

Altamimi Z, Rebischung P, Métivier L, Collilieux X (2016) ITRF2014: A new release of the International Terrestrial Reference Frame modeling nonlinear station motions. J Geophys Res 121:6109–6131. doi: 10.1002/2016JB013098

Amaro-Mellado JL, Morales-Esteban A, Asencio-Cortés G, Martínez-Álvarez F (2017) Comparing seismic parameters for different source zone models in the Iberian Peninsula. Tectonophysics 717:449–472. doi: 10.1016/j.tecto.2017.08.032

Andeweg B (2002) Cenozoic tectonic evolution of the Iberian Peninsula: effects and causes of changing stress fields. Ph.D. Thesis, Vrije Universiteit Amsterdam,

Argus DF, Gordon RG, DeMets C (2011) Geologically current motion of 56 plates relative to the no-net-rotation reference frame. Geochemistry Geophys Geosystems 12:Q11001. doi: 10.1029/2011GC003751

Asensio E (2014) Estudios de la deformación cortical de la península ibérica mediante observaciones GPS. Ph.D. Thesis, University of Barcelona

Asensio E, Khazaradze G, Echeverria A, et al (2012) GPS studies of active deformation in the Pyrenees. Geophys J Int 190:913–921. doi: 10.1111/j.1365-246X.2012.05525.x

Badal J, Chen Y, Zhang Z (2011) Modeling of Rayleigh wave dispersion in Iberia. Geosci Front 2:35–48. doi: 10.1016/j.gsf.2010.09.004

Bennett R, Hreinsdóttir S (2007) Constraints on vertical crustal motion for long baselines in the central Mediterranean region using continuous GPS. Earth Planet Sci Lett 275(3-4):419–434. doi: 10.1016/j.epsl.2007.03.008

Blewitt G (1997) Basics of the GPS Technique: Observation Equations. In: Johnson B (ed) Geodetic Applications of GPS. Nordic Geodetic Commission, Sweden, pp 10–54

Blewitt G, Lavallée D (2002) Effect of annual signals on geodetic velocity. J Geophys Res 107:2145--. doi: 10.1029/2001JB000570

Buforn E, Bezzeghoud M, Udías A, Pro C (2004) Seismic Sources on the Iberia-African Plate Boundary and their Tectonic Implications. Pure Appl Geophys 161:623–646. doi: 10.1007/s00024-003-2466-1

Buforn E, Pro C, Cesca S, et al (2011) The 2010 Granada, Spain, Deep Earthquake. Bull Seismol Soc Am 101:2418–2430. doi: 10.1785/0120110022

Cabral J, Mendes VB, Figueiredo P, et al (2017) Active tectonics in Southern Portugal (SW Iberia) inferred from GPS data. Implications on the regional geodynamics. J Geodyn 112:1–11. doi: 10.1016/j.jog.2017.10.002

Cardozo N, Allmendinger RW (2009) SSPX: A program to compute strain from displacement/velocity data. Comput Geosci 35:1343–1357. doi: 10.1016/j.cageo.2008.05.008

Cenni N, Viti M, Mantovani E (2015) Space geodetic data (GPS) and earthquake forecasting: Examples from the Italian geodetic network. Boll di Geofis Teor ed Appl 56:129–150. doi: 10.4430/bgta0139

de Jong K (1990) Alpine tectonics and rotation pole evolution of Iberia. Tectonophysics 184:279–296. doi: 10.1016/0040-1951(90)90444-D

de Vicente G, Cloetingh S, Muñoz-Martín A, et al (2008) Inversion of moment tensor focal mechanisms for active stresses around the microcontinent Iberia: Tectonic implications. Tectonics 27:1–22. doi: 10.1029/2006TC002093

DeMets C, Gordon RG, Argus DF, Stein S (1994) Effect of recent revisions to the geomagnetic reversal time scale on estimates of current plate motions. 21:2191–2194

Echeverria A (2015) GPS present-day kinematics of the eastern Betics, Spain. Ph.D. Thesis, Universitat de Barcelona

Echeverria A, Khazaradze G, Asensio E, et al (2013) Crustal deformation in eastern Betics from CuaTeNeo GPS network. Tectonophysics 608:600–612. doi: 10.1016/j.tecto.2013.08.020

Echeverria A, Khazaradze G, Asensio E, Masana E (2015) Geodetic evidence for continuing tectonic activity of the Carboneras fault (SE Spain). Tectonophysics 663:302–309. doi: 10.1016/j.tecto.2015.08.009

Estey LH, Meertens CM, Uti S (1999) TEQC: The Multi-Purpose Toolkit for GPS/GLONASS Data. GPS Solut 3:42–49

Fernandes RMS, Ambrosius BAC, Noomen R, et al (2003) The relative motion between Africa and Eurasia as derived from ITRF2000 and GPS data. Geophys Res Lett 30:1–5. doi: 10.1029/2003GL017089

Fernandes RMS, Miranda JM, Meijninger BML, et al (2007) Surface velocity field of the Ibero-Maghrebian segment of the Eurasia-Nubia plate boundary. Geophys J Int 169:315–324. doi: 10.1111/j.1365-246X.2006.03252.x

Frontera T, Concha A, Blanco P, et al (2012) DInSAR Coseismic Deformation of the May 2011Mw 5.1 Lorca Earthquake (southeastern Spain). Solid Earth 3:111–119. doi: 10.5194/se-3-111-2012

Garate J, Martin-Davila J, Khazaradze G, et al (2015) Topo-Iberia Project: CGPS crustal velocity field in the Iberian Peninsula and Morocco. GPS Solut 19:187–295. doi: 10.1007/s10291-014-0387-3

García-Mayordomo J (2015) CREACIÓN de un modelo de zonas sismogénicas para el cálculo del mapa de peligrosidad sísmica de España. Instituto Geológico y Minero de España, Madrid, Spain

Giaconia F, Booth-Rea G, Ranero CR, et al (2015) Compressional tectonic inversion of the Algero-Balearic basin: Latemost Miocene to present oblique convergence at the Palomares margin (Western Mediterranean). Tectonics 34:1516–1543. doi: 10.1002/2015TC003861

González PJ, Tiampo KF, Palano M, et al (2012) The 2011 Lorca earthquake slip distribution controlled by groundwater crustal unloading. Nat Geosci 5:821–825. doi: 10.1038/NGEO1610

Herraiz M, De Vicente G, Lindo-Ñaupari R, et al (2000) The recent (upper Miocene to Quaternary) and present tectonic stress distributions in the Iberian Peninsula. Tectonics 19(4):762–786

Herring T (2003) MATLAB Tools for viewing GPS velocities and time series. GPS Solut 7:194–199. doi: 10.1007/s10291-003-0068-0

Herring T, King RW, Mcclusky S. C (2008) Introduction to GAMIT/GLOBK. Cambridge, MA, USA

Hofmann-Wellenhof B, Lichtenegger H, Wasle E (2008) GNSS: Global Navigation Satellite Systems: GPS, GLONASS, Galileo and more. SpringerWienNewYork, Wien (Austria)

Jeffrey C (2010) An introduction to GNSS: GPS, GLONASS, Galileo and other Global Navigation Satellite Systems. NovAtel Inc.

Khazaradze G, Echeverria A, Asensio E (2014a) Present-day crustal deformation field of the Iberian Peninsula estimated by GPS measurements. Física la Tierra 26:35–46. doi: 10.5209/rev_FITE.2014.v26.46970

Khazaradze G, Echeverria A, Asensio E, McCaffrey R (2014b) Elastic block model for the Betic-Rif Arc from inversion of GPS data Tectonic setting. Geophys Res Abstr 16:EGU2014-1630–2

Koulali A, Ouazar D, Tahayt A, et al (2011) New GPS constraints on active deformation along the Africa-Iberia plate boundary. Earth Planet Sci Lett 308:211–217. doi: 10.1016/j.epsl.2011.05.048

López-Fernández C, Pulgar JA, Gallart J, et al (2008) Zonación sismotectónica del NO de la Península Ibérica. Geo-Temas 10:

Martínez-Díaz JJ, Álvarez-Gómez JA, García-Mayordomo J, et al (2012) Interpretación tectónica de la fuente del terremoto de Lorca de 2011 (Mw 5,2) y sus efectos superficiales. Boletín Geológico y Min 2011:441–458

Martínez-Díaz JJ, Hernández-Enrile JL (1992) Geometría y cinemática de la zona de cizallamiento Lorca-Totana (Falla de Alhama de Murcia). In: III Congreso Geológico de España y VII Congreso Latinoamericano de Geología. Simposios Tomo 2, Salamanca, pp 420–430

Martínez-Díaz JJ, Hernández-Enrile JL (2004) Neotectonics and morphotectonics of the southern Almería region (Betic Cordillera-Spain) kinematic implications. Int J Earth Sci 93:189–206. doi: 10.1007/s00531-003-0379-y

Masana E, Martínez-Díaz JJ, Hernández-Enrile JL, Santanach P (2004) The Alhama de Murcia fault (SE Spain), a seismogenic fault in a diffuse plate boundary: Seismotectonic implications for the Ibero-Magrebian region. J Geophys Res 109:1–17. doi: 10.1029/2002JB002359

McClusky S, Reilinger R, Mahmoud S, et al (2003) GPS constraints on Africa (Nubia) and Arabia plate motions. Geophys J Int 155:126–138. doi: 10.1046/j.1365-246X.2003.02023.x

Mezcua J, Rueda J, Garcia Blanco RM (2013) Iberian Peninsula Historical Seismicity Revisited: An Intensity Data Bank. Seismol Res Lett 84:9–18. doi: 10.1785/0220120097

Moreno X (2011) Neotectonic and Paleoseismic onshore-offshore integrated study of the Carboneras Fault (Eastern Betics, SE Iberia). Ph.D. Thesis, University of Barcelona

Nguyen HN, Vernant P, Mazzotti S, et al (2016) 3-D GPS velocity field and its implications on the present-

day post-orogenic deformation of the Western Alps and Pyrenees. Solid Earth 7:1349–1363. doi: 10.5194/se-7-1349-2016

Nocquet J-M, Calais E (2004) Geodetic Measurements of Crustal Deformation in the Western Mediterranean and Europe. Pure Appl Geophys 161:661–681. doi: 10.1007/s00024-003-2468-z

Ozener H, Dogru A, Unlutepe A (2009) An approach for rapid assessment of seismic hazards in turkey by continuous GPS data. Sensors 9:602–615. doi: 10.3390/s90100602

Palano M, González PJ, Fernández J (2015) The Diffuse Plate boundary of Nubia and Iberia in the Western Mediterranean: Crustal deformation evidence for viscous coupling and fragmented lithosphere. Earth Planet Sci Lett 430:439–447. doi: 10.1016/j.epsl.2015.08.040

Palano M, González PJ, Fernández J (2013) Strain and stress fi elds along the Gibraltar Orogenic Arc : Constraints on active geodynamics. Gondwana Res 23:1071–1088. doi: 10.1016/j.gr.2012.05.021

Rigo A, Béjar-Pizarro M, Martínez-Díaz JJ (2013) Monitoring of Guadalentín valley (southern Spain) through a fast SAR Interferometry method. J Appl Geophys 91:39–48. doi: 10.1016/j.jappgeo.2013.02.001

Rosenbaum G, Lister GS, Duboz C (2002) Relative motions of Africa, Iberia and Europe during Alpine orogeny. Tectonophysics 359:117–129. doi: 10.1016/S0040-1951(02)00442-0

Sanz de Galdeano C (2000) Evolution of Iberia during the Cenozoic with special emphasis on the formation of the Betic Cordillera and its relation with the western Mediterranean. In: 1º Congresso sobre o Cenozóico de Portugal. Lisboa, pp 9–24

Savostin LA, Sibuet J-C, Zonenshain LP, et al (1986) Kinematic evolution of the Tethys belt from the Atlantic Ocean to the Pamir since the Triassic. Tectonophysics 123:1–35. doi: 10.1016/0040-1951(86)90192-7

Serpelloni E, Faccenna C, Spada G, et al (2013) Vertical GPS ground motion rates in the Euro-Mediterranean region: New evidence of velocity gradients at different spatial scales along the Nubia-Eurasia plate boundary. J Geophys Res Solid Earth 118:6003–6024. doi: 10.1002/2013JB010102

Serpelloni E, Vannucci G, Pondrelli S, et al (2007) Kinematics of the Western Africa-Eurasia plate boundary from focal mechanisms and GPS data. Geophys J Int 169:1180–1200. doi: 10.1111/j.1365-246X.2007.03367.x

Srivastava SP, Roest WR, Kovacs LC, et al (1990) Motion of Iberia since the Late Jurassic: Results from detailed aeromagnetic measurements in the Newfoundland Basin. Tectonophysics 184:229–260

Stich D, Ammon CJ, Morales J (2003) Moment tensor solutions for small and moderate earthquakes in the Ibero-Maghreb region. J Geophys Res Solid Earth 108:. doi: 10.1029/2002JB002057

Stich D, Martín R, Morales J (2010) Moment tensor inversion for Iberia-Maghreb earthquakes 2005-2008. Tectonophysics 483:390–398. doi: 10.1016/j.tecto.2009.11.006

Stich D, Serpelloni E, Mancilla F, et al (2006) Kinematics of the Iberia-Maghreb plate contact from seismic moment tensors and GPS observations. Tectonophysics 426:295–317. doi: 10.1016/j.tecto.2006.08.004

Tagliaferro M (2017) Estudio comparativo de deformación usando técnicas geodésicas y teledetección de la cuenca Guadalentín (Murcia, España). Master's Thesis, Universitat de Barcelona

Vera JA (2004) Geología de España. Madrid, Sociedad Geológica de España-Instituto Geológico y Minero de España, 884 pp

Vergés J, Fernàndez M (2012) Tethys-Atlantic interaction along the Iberia-Africa plate boundary: The Betic-Rif orogenic system. Tectonophysics 579:144–172. doi: 10.1016/j.tecto.2012.08.032

Vernant P, Fadil A, Mourabit T, et al (2010) Geodetic constraints on active tectonics of the Western Mediterranean: Implications for the kinematics and dynamics of the Nubia-Eurasia plate boundary zone. J Geodyn 49:123–129. doi: 10.1016/j.jog.2009.10.007

Vernant P, Hivert F, Chéry J, et al (2013) Erosion-induced isostatic rebound triggers extension in low convergent mountain ranges. Geology 41:467–470. doi: 10.1130/G33942.1

APPENDIX

The appendix of this thesis is attached in the end. It consists of four sections:

A1. CGPS networks of the Iberian Peninsula. A description of the continuous GPS networks used in this study is provide.

A2. GAMIT/GLOBK parameters used in the processing.

A3. Table with the three components of the velocity field for each station.

A4. Horizontal velocity field and velocity domain interpretation.

A5. Vertical velocity field.

Digital support with the Appendix